15 April 2002

ELSEVIER

Optics Communications 205 (2002) 163–186

OPTICS COMMUNICATIONS

www.elsevier.com/locate/optcom

Raman-enhanced polarization beats in Markovian stochastic fields

Yanpeng Zhang[a,b,*], Chenli Gan[a], Keqing Lu[b], Chuangshe Li[b], Xun Hou[b]

[a] *Department of Physics, University of Connecticut, U-3046, Storrs, CT 06269, USA*
[b] *Department of Electronic Science and Technology, Xi'an Jiaotong University, Xi'an 710049, China*

Received 30 October 2001; received in revised form 2 January 2002; accepted 14 February 2002

Abstract

Raman-enhanced polarization beats (REPBs) with broadband noisy light are investigated using chaotic field, phase-diffusion, and Gaussian-amplitude models. The polarization beat signal is shown to be particularly sensitive to the statistical properties of the Markovian stochastic light fields with arbitrary bandwidth. Different stochastic models of the laser field only affect the sixth- and fourth-order coherence functions. The interferometric contrast ratio is equally sensitive to the amplitude and phase fluctuations of the Markovian stochastic fields. The constant background of the beat signal originates from the amplitude fluctuation. The Gaussian-amplitude field shows fluctuations larger than the chaotic field, which again exhibits fluctuations much larger than for the phase-diffusion field with pure phase fluctuations caused by spontaneous emission. It is also found that the beat signal oscillates not only temporally but also spatially, and the temporal period corresponds to the Raman frequency shift of 655.7 cm^{-1}. The overall accuracy of using REPB to measure the Raman resonant frequency is determined by the relaxation rates of the Raman mode and the molecular-reorientational grating. It is worth mentioning that the asymmetric behaviors of the polarization beat signals due to the unbalanced dispersion effects between two arms of interferometer do not affect the overall accuracy in case using REPB to measure the Raman resonant frequency, and different colors are optimally correlated at different values of the interferometric delay.

PACS: 42.65.Dr; 42.65.Hw

1. Introduction

The atomic response to Markovian stochastic optical fields is now largely well understood [1–10]. When the laser field is sufficiently intense that many photon interactions occur, the laser spectral bandwidth or spectral shape, obtained from the second-order correlation function, is inadequate to characterize the field. Rather than using higher-order correlation functions explicitly, three different Markovian fields are

* Corresponding author. Fax: +1-860-486-3346.
E-mail address: ypgzhang@phys.uconn.edu (Y. Zhang).

0030-4018/02/$ - see front matter
PII: S0030-4018(02)01308-1

considered in these studies: (a) the chaotic field, (b) the phase-diffusion field, and (c) the Gaussian-amplitude field. The chaotic field undergoes both amplitude and phase fluctuations and corresponds to a multimode laser field with a large number of uncorrelated modes, or a single-mode laser emitting light below threshold. Since a chaotic field does not possess any intensity stabilization mechanism, the field can take on any value in a two-dimensional region of the complex plane centered about the origin. The phase-diffusion field undergoes only phase fluctuations and corresponds to an intensity-stabilized single-mode laser field. The phase of the laser field, however, has no natural stabilizing mechanism. The Gaussian-amplitude field undergoes only amplitude fluctuations. Although pure amplitude fluctuations cannot be produced by a nonadiabatic process, we do consider the Gaussian-amplitude field for two reasons. First, because it allows us to isolate those effects due solely to amplitude fluctuations and second, because it is an example of a field which undergoes stronger amplitude (intensity) fluctuations than a chaotic field. By comparing the results for the chaotic and the Gaussian-amplitude fields we can determine the effect of increasing amplitude fluctuations [1–5].

This paper addresses the role of noise in the incident fields on the nature of the wave-mixing signal-particularly in the time domain. This important topic has been already treated extensively in the literature including the introduction of a new diagrammatic technique (called factorized time correlator diagrams) [11–14]. They have treated the higher order noise correlators when circular Gaussian statistics apply. There should be two classes of such two component beams. In one class the components are derived from separate lasers and their mixed (cross) correlators should vanish. In the second case the two components are derived from a single laser source whose spectral output is doubly peaked. This can be created from a single dye laser in which two different dyes in solution together are amplified [11–13]. The present paper deals only with the first class. That is to say, we are considering only the class of two-color beams in which each color is derived from a separate broadband laser source. The doubled peaked beams 1 and 2 (Fig. 1) are paired and correlated, but each of the peaks is uncorrelated. Beam3, having one of the peaks (from a same broadband laser source) found in beams 1 and 2 is dependent and correlated to beams 1 and 2. In any case the literature has already explored both theoretically and experimentally the use of such multicolor noisy light in four-wave mixing (FWM). Interestingly, that work only treats the second class of multicolored beams (a single laser source for the multipeaked ''tailored'' light) in self-diffraction geometry [11–14]. Also that work did not treat the Raman-enhanced polarization beats (REPB) with phase-conjugation geometry using three types of noisy models and furthermore its beam 3 was not noisy (it was ''monochromatic'').

The chaotic field, the Brownian-motion phase-diffusion field, and the Gaussian-amplitude field are considered in parallel with a discussion on REPB. We develop an unified theory which involves sixth-order coherence-function to study the influence of partial-coherence properties of light field on polarization beats. Polarization beats, which originate from the interference between the macroscopic polarizations, have attracted a lot of attention recently [15–22]. It is closely related to quantum beats, Raman quantum beats [16], or coherent Raman spectroscopy (CRS). CRS has become a powerful tool for studying the vibrational or rotational mode of a molecule. The most commonly used coherent Raman spectroscopy is coherent anti-Stokes Raman scattering (CARS) and Raman-induced Kerr effect spectroscopy. Recently

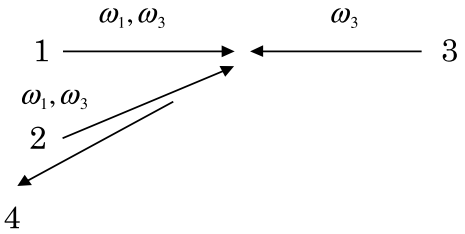

Fig. 1. Schematic diagram of the geometry of REPB.

Raman-enhanced nondegenerate four-wave mixing (RENFWM) has attracted much attention [23–26]. RENFWM is a third-order nonlinear phenomenon with phase-conjugation geometry. It over conventional CARS possesses the advantages of nonresonant background suppression, excellent spatial resolution even for the case of small Raman shifts, free choice of interaction volume, and simple optical alignment. Furthermore, since the phase matching condition is not critical in RENFWM, it possesses a large frequency bandwidth and is therefore suitable for studying subpicosecond relaxation processes which have broad resonant linewidth. Fu et al. has performed time-delayed RENFWM with incoherent light to measure the vibrational dephasing time [24]. They also found an enhancement of the ratio between the resonant and nonresonant RENFWM signal intensities as the time delay was increased when the laser had broadband linewidth [25]. One of the relevant problems is the FWM with broadband noisy light, which was proposed by Morita et al. [27] to achieve an ultrafast temporal resolution of relaxation processes. Since they assumed that laser linewidth is much longer than transverse relaxation rate, their theory cannot be used to study the effect of the light bandwidth on the Bragg reflection signal. Asaka et al. [28] considered the finite linewidth effect. However, the constant background contribution has been ignored in their analysis. Our higher-order correlation on polarization beats includes the finite light bandwidth effect, constant background contribution, light field fluctuations and controllable unbalance dispersive effects [11,14]. These are of vital importance in the REPB.

2. Basic theory

REPB is a third-order nonlinear polarization beat phenomenon. The basic geometry is shown in Fig. 1. Beams 1 and 2 consist of two central circular frequency components ω_1 and ω_3, a small angle exists between them. Beam 3 with central circular frequency ω_3 is almost propagating along the opposite direction of beam 1. In a Kerr medium, the nonlinear interaction of beams 1 and 2 with the medium gives rise to two molecular-reorientational gratings, i.e., ω_1 and ω_3 will induce their own static gratings G1 and G2, respectively. The FWM signal is the result of the diffraction of beam 3 by G1 and G2.

Now, if $|\omega_1 - \omega_3|$ is near the Raman resonant frequency Ω_R, a large angle moving grating and two small angle moving gratings formed by the interference of beams 2, 3 and beams 1, 2, respectively, will excite the Raman-active vibrational mode of the medium and enhance the FWM signal.The beat signal (beam 4) is along the opposite direction of beam 2 approximately.

The complex electric fields of beam 1, E_{p1}, and beam 2, E_{p2}, can be written as

$$\begin{aligned} E_{p1} &= E_1(\vec{r},t) + E_2(\vec{r},t) = A_1(\vec{r},t)\exp(-\mathrm{i}\omega_1 t) + A_2(\vec{r},t)\exp(-\mathrm{i}\omega_3 t) \\ &= \varepsilon_1 u_1(t)\exp\left[\mathrm{i}\left(\vec{k}_1\cdot\vec{r}-\omega_1 t\right)\right] + \varepsilon_2 u_3(t)\exp\left[\mathrm{i}\left(\vec{k}_2\cdot\vec{r}-\omega_3 t\right)\right], \end{aligned} \tag{1}$$

$$\begin{aligned} E_{p2} &= E_1'(\vec{r},t) + E_2'(\vec{r},t) = A_1'(\vec{r},t)\exp(-\mathrm{i}\omega_1 t) + A_2'(\vec{r},t)\exp(-\mathrm{i}\omega_3 t) \\ &= \varepsilon_1' u_1(t-\tau+\delta\tau)\exp\left[\mathrm{i}\left(\vec{k}_1'\cdot\vec{r}-\omega_1 t+\omega_1\tau-\omega_1\delta\tau\right)\right] \\ &\quad + \varepsilon_2' u_3(t-\tau)\exp\left[\mathrm{i}\left(\vec{k}_2'\cdot\vec{r}-\omega_3 t+\omega_3\tau\right)\right]. \end{aligned} \tag{2}$$

Here, ε_i, $\vec{k}_i(\varepsilon_i', \vec{k}_i')$ are the constant field amplitude and the wave vector of frequency components ω_1 and ω_3 in beam 1 (beam 2), respectively. $u_i(t)$ is a dimensionless statistical factor that contains phase and amplitude fluctuations. We assume that the ω_1 (ω_3) component of E_{p1} and E_{p2} comes from a single laser source and τ is the time delay of beam 2 with respect to beam 1. $\delta\tau$ denotes the difference between two autocorrelation processes in the zero time delay ($\delta\tau > 0$). On the other hand, the complex electric fields of beam 3 can be written as

$$E_{p3} = A_3(\vec{r},t)\exp(-\mathrm{i}\omega_3 t) = \varepsilon_3 u_3(t)\exp\left[\mathrm{i}\left(\vec{k}_3\cdot\vec{r}-\omega_3 t\right)\right]. \tag{3}$$

Here, ω_3, ε_3, and $\vec{k}_3$ are the frequency, the field amplitude and the wave vector of the field, respectively.

Different colors correlate at different delay times because they have been delayed in the dispersed beam relative to the undispersed beam. This is analogous to the stretching of short pulses by transmission through a dispersive medium (chirp). In fact, identical physical processes are responsible for chirp in coherent short pulses and the correlation functions of broadband fields. Considering the situation in which the double frequencies noisy field derived from separate lasers with a finite bandwidth is split into twin replicas; then one of twin fields, E_{p2}, is transmitted through a dispersive medium so that it is no longer identical to the other E_{p1}. Two autocorrelations corresponding to static gratings G1 and G2, respectively, are differently stretched in τ because each color component between beams 1 and 2 is maximally correlated at different time delay times, whereas in beam 1 or beam 2 all color components are maximally correlated at the same delay time. The phases of chirped correlation functions exhibit a time dependence that is similar to the time-dependent phases of chirped coherent short pulses. Unchirped (transform-limited) correlation functions and short pulses have phases that are independent of time. An important practical distinction between short pulses and noisy-light correlation functions is that the chirping of correlation functions in double-frequency noisy-light interferometry can occur only after the double-frequency noisy field is split into beams 1 and 2, and then only if there is a difference between the dispersion in the paths traveled by beams 1 and 2, but a short pulse is chirped as it propagates through any dispersive medium between the source and the sample. That is to say, ultrashort pulses of equivalent bandwidth are not immune to such dispersive effects (even when balanced) because the transform limited light pulse is in fact temporally broadened (it is chirped) and this has drastic effects on its time resolution (the auto-correlation). In this sense the REPB with double-frequency noisy light has an advantage [11].

The order parameters Q_1 and Q_2 of two static gratings induced by beams 1 and 2 satisfy the following equations [23–26]:

$$\frac{\mathrm{d}Q_1}{\mathrm{d}t} + \gamma Q_1 = \chi\gamma E_1(\vec{r},t)\left[E_1'(\vec{r},t)\right]^*, \tag{4}$$

$$\frac{\mathrm{d}Q_2}{\mathrm{d}t} + \gamma Q_2 = \chi\gamma E_2(\vec{r},t)\left[E_2'(\vec{r},t)\right]^*. \tag{5}$$

Here γ and χ are the relaxation rate and the nonlinear susceptibility of the two static gratings, respectively.

We consider a large angle moving grating (the order parameter Q_{R1}) and two small angle moving gratings (the order parameters Q_{R2}, Q_{R3}) formed by the interference of beams 2, 3 and beams 1, 2, respectively. The order parameters Q_{R1}, Q_{R2}, Q_{R3} satisfy the following equations:

$$\frac{\mathrm{d}Q_{R1}}{\mathrm{d}t} + (\gamma_\mathrm{R} - \mathrm{i}\Delta)Q_{R1} = \frac{\mathrm{i}\alpha_\mathrm{R}}{4\hbar}\left[A_1'(\vec{r},t)\right]^* A_3(\vec{r},t), \tag{6}$$

$$\frac{\mathrm{d}Q_{R2}}{\mathrm{d}t} + (\gamma_\mathrm{R} - \mathrm{i}\Delta)Q_{R2} = \frac{\mathrm{i}\alpha_\mathrm{R}}{4\hbar}A_1(\vec{r},t)\left[A_2'(\vec{r},t)\right]^*, \tag{7}$$

$$\frac{\mathrm{d}Q_{R3}}{\mathrm{d}t} + (\gamma_\mathrm{R} - \mathrm{i}\Delta)Q_{R3} = \frac{\mathrm{i}\alpha_\mathrm{R}}{4\hbar}\left[A_1'(\vec{r},t)\right]^* A_2(\vec{r},t). \tag{8}$$

Here $\Delta = |\omega_1 - \omega_3| - \Omega_\mathrm{R}$ is the frequency detuning; Ω_R and γ_R are the resonant frequency and the relaxation rate of the Raman mode, respectively. α_R is a parameter denoting the strength of the Raman interaction.

The induced five third-order nonlinear polarizations which are responsible for the FWM signals are

$$\begin{aligned} P_1 &= Q_1(\vec{r},t)E_3(\vec{r},t) \\ &= \chi\gamma\varepsilon_1\left(\varepsilon_1'\right)^*\varepsilon_3\exp\left\{\mathrm{i}\left[\left(\vec{k}_1-\vec{k}_1'+\vec{k}_3\right)\cdot\vec{r}-\omega_3 t-\omega_1(\tau-\delta\tau)\right]\right\} \\ &\quad\times\int_0^\infty u_1(t-t')u_1^*(t-t'-\tau+\delta\tau)u_3(t)\exp(-\gamma t')\,\mathrm{d}t', \end{aligned} \tag{9}$$

$$\begin{aligned} P_2 &= Q_2(\vec{r},t)E_3(\vec{r},t) \\ &= \chi\gamma\varepsilon_2\left(\varepsilon_2'\right)^*\varepsilon_3\exp\left\{\mathrm{i}\left[\left(\vec{k}_2-\vec{k}_2'+\vec{k}_3\right)\cdot\vec{r}-\omega_3 t-\omega_3\tau\right]\right\}\int_0^\infty u_3(t-t')u_3^*(t-t'-\tau)u_3(t)\exp(-\gamma t')\,\mathrm{d}t', \end{aligned} \tag{10}$$

$$\begin{aligned} P_{R1} &= \frac{1}{2}N\alpha_{\mathrm{R}}Q_{R1}(\vec{r},t)E_1(\vec{r},t)\exp[\mathrm{i}(\omega_1-\omega_3)t-\mathrm{i}\omega_1(\tau-\delta\tau)] \\ &= \mathrm{i}\chi_{\mathrm{R}}\gamma_{\mathrm{R}}\varepsilon_1\left(\varepsilon_1'\right)^*\varepsilon_3\exp\left\{\mathrm{i}\left[\left(\vec{k}_1-\vec{k}_1'+\vec{k}_3\right)\cdot\vec{r}-\omega_3 t-\omega_1(\tau-\delta\tau)\right]\right\} \\ &\quad\times\int_0^\infty u_1(t)u_1^*(t-t'-\tau+\delta\tau)u_3(t-t')\exp[-(\gamma_{\mathrm{R}}-\mathrm{i}\Delta)]\,\mathrm{d}t', \end{aligned} \tag{11}$$

$$\begin{aligned} P_{R2} &= \frac{1}{2}N\alpha_{\mathrm{R}}Q_{R2}(\vec{r},t)E_3(\vec{r},t)\exp[\mathrm{i}(\omega_3-\omega_1)t-\mathrm{i}\omega_3\tau] \\ &= \mathrm{i}\chi_{\mathrm{R}}\gamma_{\mathrm{R}}\varepsilon_1\left(\varepsilon_2'\right)^*\varepsilon_3\exp\left\{\mathrm{i}\left[\left(\vec{k}_1-\vec{k}_2'+\vec{k}_3\right)\cdot\vec{r}-\omega_1 t-\omega_3\tau\right]\right\} \\ &\quad\times\int_0^\infty u_1(t-t')u_3^*(t-t'-\tau)u_3(t)\exp[-(\gamma_{\mathrm{R}}-\mathrm{i}\Delta)]\,\mathrm{d}t', \end{aligned} \tag{12}$$

$$\begin{aligned} P_{R3} &= \frac{1}{2}N\alpha_{\mathrm{R}}Q_{R3}(\vec{r},t)E_3(\vec{r},t)\exp[\mathrm{i}(\omega_1-\omega_3)t-\mathrm{i}\omega_1(\tau-\delta\tau)] \\ &= \mathrm{i}\chi_{\mathrm{R}}\gamma_{\mathrm{R}}\left(\varepsilon_1'\right)^*\varepsilon_2\varepsilon_3\exp\left\{\mathrm{i}\left[\left(\vec{k}_2-\vec{k}_1'+\vec{k}_3\right)\cdot\vec{r}-(2\omega_3-\omega_1)t-\omega_1(\tau-\delta\tau)\right]\right\} \\ &\quad\times\int_0^\infty u_1^*(t-t'-\tau+\delta\tau)u_3(t-t')u_3(t)\exp[-(\gamma_{\mathrm{R}}-\mathrm{i}\Delta)]\,\mathrm{d}t', \end{aligned} \tag{13}$$

with $\chi_{\mathrm{R}}=N\alpha_{\mathrm{R}}^2/8\hbar\gamma_{\mathrm{R}}$ and N the density of molecules.

3. The chaotic field

We have the total third-order polarization $P^{(3)}=P_1+P_2+P_{R1}+P_{R2}+P_{R3}$. For the macroscopic system where phase matching takes place this signal must be drawn from the $P^{(3)}$ developed on one chromophore multiplied by the $(P^{(3)})^*$ that is developed on another chromophore which must be located elsewhere in space (with summation over all such pairs) [11–14]. In general, the signal is homodyne (quadrature) detected. This means that the signal at the detector is derived from the squared modulus of the sum of all of the fields that are generated from the huge number of polarized chromophores in the interaction volume. The sum over chromophores leads to the phase-matching condition at the signal level and its square modulus (the signal) is fully dominated by the bichromophoric cross terms. Thus the quadrature detected signal is effectively built from the products of all polarization fields derived from all pairs of chromophores. This bichromophoric model is particularly important to the noisy light spectroscopies where the stochastic averaging at the signal level must be carried out [12,13]. The FWM signal is proportional to the average of

the absolute square of $P^{(3)}$ over the random variable of the stochastic process, so that the signal $I(\Delta,\tau)\propto\langle|P^{(3)}|^2\rangle$ contains $5\times5=25$ different terms in the sixth-, fourth- and second-order coherence function of $u_i(t)$ in phase conjugation geometry. The ultrafast modulation spectroscopy (UMS) in self-diffraction geometry is also related to the sixth-order coherence function of the incident fields [15]. We first assumed that the laser sources are chaotic fields. A chaotic field, which is used to describe a multimode laser source, is characterized by the fluctuation of both the amplitude and the phase of the field. The random functions $u_i(t)$ of the complex noisy fields are taken to obey complex Gaussian statistics with its sixth- and fourth-order coherence function satisfying [1,5]

$$\begin{aligned}&\langle u_i(t_1)u_i(t_2)u_i(t_3)u_i^*(t_4)u_i^*(t_5)u_i^*(t_6)\rangle\\&\quad=\langle u_i(t_1)u_i^*(t_4)\rangle\langle u_i(t_2)u_i(t_3)u_i^*(t_5)u_i^*(t_6)\rangle+\langle u_i(t_1)u_i^*(t_5)\rangle\langle u_i(t_2)u_i(t_3)u_i^*(t_4)u_i^*(t_6)\rangle\\&\qquad+\langle u_i(t_1)u_i^*(t_6)\rangle\times\langle u_i(t_2)u_i(t_3)u_i^*(t_4)u_i^*(t_5)\rangle,\quad i=1,3\end{aligned}\tag{14}$$

and

$$\langle u_i(t_1)u_i(t_2)u_i^*(t_3)u_i^*(t_4)\rangle=\langle u_i(t_1)u_i^*(t_3)\rangle\langle u_i(t_2)u_i^*(t_4)\rangle+\langle u_i(t_1)u_i^*(t_4)\rangle\langle u_i(t_2)u_i^*(t_3)\rangle.\tag{15}$$

All higher order coherence functions can be expressed in terms of products of second-order coherence functions. Thus any given $2n$ order coherence function may be decomposed into the sum of $n!$ terms, each consisting of the products of n second-order coherence function.

Furthermore assuming that laser sources have Lorentzian line shape, then we have

$$\langle u_i(t_1)u_i^*(t_2)\rangle=\exp(-\alpha_i|t_1-t_2|).\tag{16}$$

Here $\alpha_i=\frac{1}{2}\delta\omega_i$, $\delta\omega_i$ is the linewidth of the laser with frequency ω_i.

We first consider the situation when the linewidths of the laser sources in beams 1, 2 and 3 are broadband (i.e., $\alpha_1,\alpha_3\gg\gamma,\gamma_R$). The composite noisy beam 1 (beam 2) is treated as one whose spectrum is simply a sum of two Lorentzians. In this limit, after performing the tedious integration we obtain for:

(i) $\tau>\delta\tau$

$$\begin{aligned}I(\Delta,\tau)\propto{}&\left(1+\eta_1^2+\eta_2^2\right)\frac{\chi_R^2\gamma_R(\alpha_1+\alpha_3)}{(\alpha_1+\alpha_3)^2+\Delta^2}-\chi_R\chi\gamma_R\gamma\frac{\Delta[(5\alpha_1+\alpha_3)(\alpha_1+\alpha_3)+\Delta^2]}{\alpha_1\left[(\alpha_1+\alpha_3)^2+\Delta^2\right]^2}+\frac{\chi^2\gamma}{2\alpha_1\alpha_3}\left(\alpha_1\eta_1^2\eta_2^2+\alpha_3\right)\\&+\left\{\frac{\chi_R^2\gamma_R^2(\alpha_1+\alpha_3)}{\alpha_1\left[(\alpha_1+\alpha_3)^2+\Delta^2\right]}-\frac{2\chi_R\chi\gamma_R\Delta}{(\alpha_1+\alpha_3)^2+\Delta^2}+\chi^2\right\}\exp(-2\alpha_1|\tau-\delta\tau|)\\&+\eta_2^2\left\{\frac{\chi_R^2\gamma_R^2(\alpha_1+\alpha_3)}{\alpha_3[(\alpha_1+\alpha_3)^2+\Delta^2]}+\chi^2\eta_1^2\right\}\exp(-2\alpha_3|\tau|)+4\eta_1\eta_2\exp(-\alpha_1|\tau-\delta\tau|-\alpha_3|\tau|)\\&\times\left\{\left[\frac{\chi^2}{2}-\frac{\chi\chi_R\gamma_R\Delta}{2\left[(\alpha_1+\alpha_3)^2+\Delta^2\right]}\right]\cos[\Delta\vec{k}\cdot\vec{r}-(\omega_1-\omega_3)\tau+\omega_1\delta\tau]\right.\\&\left.-\frac{\chi\chi_R\gamma_R(\alpha_1+\alpha_3)}{2[(\alpha_1+\alpha_3)^2+\Delta^2]}\sin\left[\Delta\vec{k}\cdot\vec{r}-(\omega_1-\omega_3)\tau+\omega_1\delta\tau\right]\right\},\end{aligned}\tag{17}$$

(ii) $0 < \tau < \delta\tau$

$$I(\Delta,\tau) \propto \left(1+\eta_1^2+\eta_2^2\right)\frac{\chi_R^2\gamma_R(\alpha_1+\alpha_3)}{(\alpha_1+\alpha_3)^2+\Delta^2} - \frac{4\chi_R\chi\gamma_R\gamma\Delta}{\alpha_1(\alpha_1+\alpha_3)^2} + \frac{\chi^2\gamma}{2\alpha_1\alpha_3}(\alpha_1\eta_1^2\eta_2^2+\alpha_3) + \chi^2\exp(-2\alpha_1|\tau-\delta\tau|)$$
$$+ 2\chi^2\eta_1^2\eta_2^2\exp(-2\alpha_3|\tau|) + \frac{\chi_R^2\gamma_R^2}{\alpha_1(\alpha_1+\alpha_3)}\exp(-2\gamma_R|\tau-\delta\tau|)$$
$$+ \frac{\chi^2}{2}\eta_1\eta_2\exp(-\alpha_1|\tau-\delta\tau|-\alpha_3|\tau|)\cos\left[\Delta\vec{k}\cdot\vec{r}-(\omega_1-\omega_3)\tau+\omega_1\delta\tau\right]$$
$$+ \chi_R\chi\gamma_R\gamma\left[\frac{1}{\gamma(\alpha_1+\alpha_3)}\exp(-\alpha_1|\tau-\delta\tau|-\alpha_3|\tau|) + \frac{1}{2\alpha_3(\alpha_1+\alpha_3)}\exp(-\alpha_3|\tau-\delta\tau|-\alpha_3|\tau|)\right]$$
$$\times\sin\left[\Delta\vec{k}\cdot\vec{r}-(\omega_1-\omega_3)\tau+\omega_1\delta\tau+\Delta|\tau-\delta\tau|\right], \tag{18}$$

and (iii) $\tau < 0$, although the beat signal modulation is complicated in general, at the tail of the signal (i.e., $|\tau| \gg \alpha_1^{-1}$, $|\tau| \gg \alpha_3^{-1}$) we have

$$I(\Delta,\tau) \propto \left(1+\eta_1^2+\eta_2^2\right)\frac{\chi_R^2\gamma_R(\alpha_1+\alpha_3)}{(\alpha_1+\alpha_3)^2+\Delta^2} - \chi_R\chi\gamma_R\gamma\frac{\Delta\left[(5\alpha_1+\alpha_3)(\alpha_1+\alpha_3)+\Delta^2\right]}{\alpha_1\left[(\alpha_1+\alpha_3)^2+\Delta^2\right]^2} + \frac{\chi^2\gamma}{2\alpha_1\alpha_3}\left(\alpha_1\eta_1^2\eta_2^2+\alpha_3\right)$$
$$+ \frac{3\chi^2\eta_1^2\eta_2^2\gamma^2}{2\alpha_3^2}\exp(-2\gamma|\tau|) + \frac{2\chi_R^2\gamma_R^2}{(\alpha_1+\alpha_3)^2}[(1+\alpha_3)\exp(-2\gamma_R|\tau|)$$
$$+ (1+\alpha_1)\eta_2^2\exp(-2\gamma_R|\tau-\delta\tau|)] + \exp(-\gamma_R|\tau-\delta\tau|-\gamma|\tau|)$$
$$\times\frac{4\eta_1\eta_2\chi\chi_R\gamma\gamma_R}{\alpha_3(\alpha_1+\alpha_3)^4}\left\{(\alpha_1+\alpha_3)(2\gamma_R+\gamma)\Delta\cos\left[\Delta\vec{k}\cdot\vec{r}-(\omega_1-\omega_3)\tau+\omega_1\delta\tau+\Delta|\tau-\delta\tau|\right]\right.$$
$$\left.-\left[(\alpha_1+2\alpha_3)(\alpha_1+\alpha_3)^2+\alpha_1\Delta^2\right]\sin\left[\Delta\vec{k}\cdot\vec{r}-(\omega_1-\omega_3)\tau+\omega_1\delta\tau+\Delta|\tau-\delta\tau|\right]\right\}. \tag{19}$$

Here, $\eta_1 = \varepsilon_2/\varepsilon_1$, $\eta_2 = \varepsilon_2'/\varepsilon_1'$ and $\Delta\vec{k} = (\vec{k}_1 - \vec{k}_1') - (\vec{k}_2 - \vec{k}_2')$.

Relation (17) consists of six terms. The sixth term depending on the $u_1(t)$ or $u_3(t)$ fourth- and second-order coherence functions is the cross-correlation intensity between five third-order nonlinear polarizations, and gives rise to the modulation of the beat signal. The interferometric contrast ratio mainly determined the modulation term is equally sensitive to the amplitude and phase fluctuations of the chaotic fields. The other terms (the τ-independent terms and the decay terms) depending on the sixth-, fourth- or second-order coherence functions of $u_1(t)$ or $u_3(t)$ are a sum of the auto-correlation intensity between five third-order nonlinear polarizations. Different stochastic models of the laser field affect only the sixth- and fourth-order coherence functions. The constant terms in relations (17)–(19), which are independent of the relative time-delay between beam 1 and beam 2, mainly originate from the amplitude fluctuation of the chaotic fields. The fourth and fifth terms in relation (17), which are shown to be particularly sensitive to the amplitude fluctuation of the chaotic fields, indicate an exponential decay of the beat signal as $|\tau|$ increases. On the other hand, REPB is different for $\tau > \delta\tau$, $0 < \tau < \delta\tau$ and $\tau < 0$ in general. However, as $|\tau| \to \infty$, Eq. (17) is identical to Eqs. (18) or (19). Physically, when $|\tau| \to \infty$, beams 1 and 2 are mutually incoherent, therefore whether τ is positive or negative does not affect the REPB.

Eq. (17) indicates that when $\tau > \delta\tau$, the temporal behavior of the beat signal intensity reflects mainly the characteristic of the lasers, i.e., the frequency $\omega_3 - \omega_1$ and the damping rate $\alpha_1 + \alpha_3$ of the modulation are determined by the incident laser beams. If we employ REPB to measure the modulation frequency $\omega_d = \omega_3 - \omega_1$, the accuracy can be improved by measuring as many cycles of the modulation as possible.

Since the amplitude of the modulation decays with a time constant $(\alpha_1 + \alpha_3)^{-1}$ as $|\tau|$ increases, the maximum domain of time delay $|\tau|$ should equal approximately $2(\alpha_1 + \alpha_3)^{-1}$. We obtain the theoretical limit of the uncertainty of the modulation frequency measurement $\Delta\omega_d$ which is $\Delta\omega_d \approx \pi(\alpha_1 + \alpha_3)$, i.e., in the modulation frequency measurement the theoretical limit of the accuracy is related to the decay time constant of the beat signal modulation amplitude. In this case, the precision of using REPB to measure the Raman resonant frequency is determined by how well $\omega_3 - \omega_1$ can be tuned to Ω_R. When $0 < \tau < \delta\tau$, Eq. (18) reflects not only the characteristic of the lasers, but also a molecule vibrational property. When $\tau < 0$, Eq. (19) indicates that beat signal modulates with a frequency $(\omega_3 - \omega_1) - \Delta = \Omega_R$ and a damping rate $\gamma_R + \gamma$ as τ is varied. We can obtain the resonant frequencies of the Raman vibrational mode with an accuracy given by $\pi(\gamma_R + \gamma)$ approximately, which is mainly determined by a molecule vibrational property.

To illustrate, Fig. 2 shows the interferograms of the beat signal intensity versus relative time delay for three different values of the reduced offset imbalance $\delta\tau$. It is noticed that as $\delta\tau$ increases, the peak-to-background contrast ratio of the interferograms diminishes. Interestingly, the phase of the fringe beating also changes sensitively to produce a variety of interferograms including asymmetric ones. $\delta\tau$ expresses the unbalance dispersion effects between the two arms. A simple realistic example is an interferometer having an effective thickness of quartz or glass that differs significantly (many mm to a few cm) between its two arms. Changing the thickness in one arm will control the degree of imbalance in the dispersion effects [11,14]. Physically, $\delta\tau$ corresponds to the separation of the peaks of the fourth and fifth terms of Eq. (17), i.e. the separation between the ω_1 only interferogram and the ω_3 only interferogram [22].

Eqs. (17)–(19) indicate that beat signal oscillates not only temporally but also spatially with a period $2\pi/\Delta k$ along the direction $\Delta\vec{k}$, which is almost perpendicular to the propagation direction of the beat signal. Here $\Delta k \approx 2\pi|\lambda_1 - \lambda_3|\theta/\lambda_3\lambda_1$, θ is the angle between beam 1 and beam 2. Physically, the polarization-beat model assumes that the pump beams are plane waves. Therefore FWM signals of two static gratings, which propagate along $\vec{k}_1 - \vec{k}_1' + \vec{k}_3$ and $\vec{k}_2 - \vec{k}_2' + \vec{k}_3$, respectively, are plane waves also. Since FWM signals propagate along slightly different direction, the interference between them leads to the spatial oscillation. Fig. 3 presents the theoretical curve of the normalized polarization beat signal intensity versus transverse distance r with fixed time delay and frequency detuning. The beat signal oscillates spatially with a period $2\pi/\Delta k = \lambda_1\lambda_3/|\lambda_1 - \lambda_3|\theta \approx 0.6$ mm, i.e., the spacing between the spatial interference fringes is 0.6 mm. To observe the spatial modulation of the beat signal the dimension of the detector should be smaller than 0.6 mm, which is not interested in our experiment.

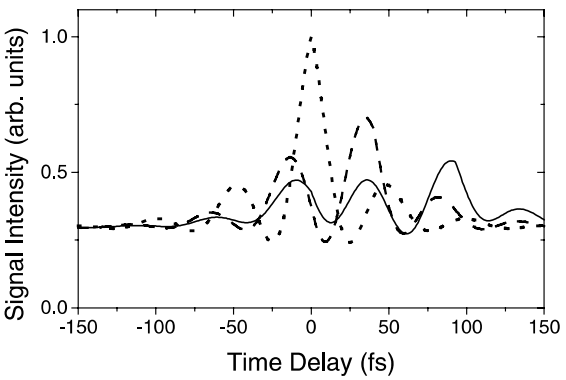

Fig. 2. The beat signal intensity versus relative time delay. The parameters are $\omega_1 = 3200$ ps^{-1}, $\omega_3 = 3324$ ps^{-1}, $\Delta k = 0$, $\eta_1 = \eta_2 = 1$, $\Delta = 0$, $\chi/\chi_R = 1$, $\gamma_R = 0.05$ ps^{-1}, $\gamma = 0.2$ ps^{-1}, $\alpha_1 = 10.8$ ps^{-1}, $\alpha_3 = 11.6$ ps^{-1}; while $\delta\tau = 0$ fs for dotted line, $\delta\tau = 43$ fs for dashed line and $\delta\tau = 100$ fs for solid line.

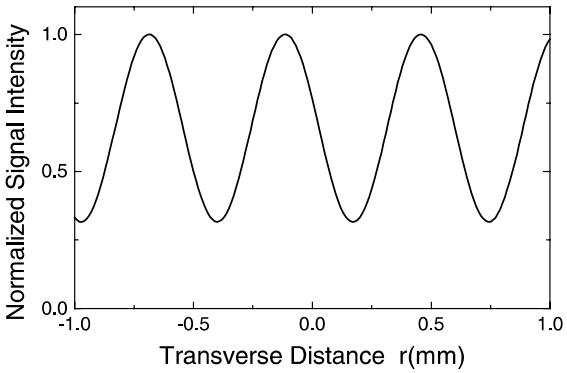

Fig. 3. Theoretical curve of the normalized polarization beat signal intensity versus transverse distance r. Parameters are $\alpha_1 = 2.7\ \mathrm{ps}^{-1}$, $\alpha_3 = 2.9\ \mathrm{ps}^{-1}$, $\tau = 0$ ps, $\delta\tau = 83$ fs, $\theta = 2.62 \times 10^{-2}$ rad, $\lambda_1 = 589$ nm, $\lambda_3 = 567$ nm, $\chi/\chi_R = 1$, $\gamma_R = 0.05\ \mathrm{ps}^{-1}$, $\gamma = 0.2\ \mathrm{ps}^{-1}$, $\eta_1 = \eta_2 = 1$, and $\Delta = 0$.

We then consider the situation when the linewidths of the laser sources in beams 1, 2 and 3 are narrow band (i.e., $\alpha_1, \alpha_3 \ll \gamma, \gamma_R$ and $\gamma_R|\tau|, \gamma|\tau| \gg 1$). In this limit, after performing the tedious integration we obtain

$$
\begin{aligned}
I(\Delta,\tau) \propto{}& \left(1+2\eta_1^2+\eta_2^2\right)\frac{\chi_R^2\gamma_R^2}{\gamma_R^2+\Delta^2} - \frac{2\chi_R\chi\gamma_R\Delta}{\gamma_R^2+\Delta^2} + \chi^2\left(1+2\eta_1^2\eta_2^2\right) + \left(\frac{\chi_R^2\gamma_R^2}{\gamma_R^2+\Delta^2} - \frac{2\chi_R\chi\gamma_R\Delta}{\gamma_R^2+\Delta^2} + \chi^2\right) \\
&\times \exp(-2\alpha_1|\tau-\delta\tau|) + \eta_2^2\left(\frac{\chi_R^2\gamma_R^2}{\gamma_R^2+\Delta^2} + 4\eta_1^2\chi^2\right)\exp(-2\alpha_3|\tau|) + 4\exp(-\alpha_1|\tau-\delta\tau| - \alpha_3|\tau|) \\
&\times \left\{\left[\chi^2 + \chi\chi_R\gamma_R\Delta\left(\frac{\alpha_3}{\gamma\gamma_R+\gamma^2+\Delta^2} + \frac{1}{\gamma_R^2+\Delta^2}\right)\right]\cos\left[\Delta\vec{k}\cdot\vec{r} - (\omega_1-\omega_3)\tau + \omega_1\delta\tau\right]\right. \\
&\left. + \eta_1\eta_2\chi\chi_R\gamma_R\left[\frac{\alpha_3(\gamma_R+\gamma)}{\gamma(\gamma_R+\gamma)^2+\Delta^2} - \frac{\gamma_R}{\gamma_R^2+\Delta^2}\right]\sin\left[\Delta\vec{k}\cdot\vec{r} - (\omega_1-\omega_3)\tau + \omega_1\delta\tau\right]\right\}. \qquad (20)
\end{aligned}
$$

This case when the pump beams have a narrow-band linewidth is similar to Eq. (17).

4. The Raman echo

It is interesting to understand the underlying physics in REPB with incoherent lights. Much attention has been paid to the study of various ultrafast phenomena by using incoherent light sources recently [11–14,22,27]. The REPB with incoherent lights is related to the three-pulse Raman echoes [23–25]. It is different from the conventional true Raman echo which is a seventh order process or the Raman pseudo-echo which is a fifth order process [29,30]. We now consider the case when the laser sources have a broadband linewidth, then

$$
\exp(-\alpha_i|t_1-t_2|) \approx \frac{2}{\alpha_i}\delta(t_1-t_2), \quad i = 1,3. \qquad (21)
$$

When we substitute Eqs. (14)–(16) and (21) into $I(\Delta,\tau)\propto\langle|P^{(3)}|^2\rangle$, we obtain, for:

(i) $\tau>\delta\tau$

$$
\begin{aligned}
I(\Delta,\tau)\propto{}&\chi_R^2\gamma_R\left[\frac{(1+\eta_1^2+\eta_2^2)}{\alpha_1+\alpha_3}+\frac{\eta_1^2\gamma_R}{\alpha_1(\gamma_R+\alpha_3)}\right]-\frac{4\chi_R\chi\gamma_R\gamma\Delta}{\alpha_1\left[(\gamma_R+\gamma+\alpha_1+\alpha_3)^2+\Delta^2\right]}\\
&+\chi^2\gamma\left[\frac{1}{2\alpha_1}+\frac{\eta_1^2\eta_2^2(3\gamma+\alpha_3)}{2\alpha_3(\gamma+\alpha_3)}\right]+\chi^2\exp(-2\alpha_1|\tau-\delta\tau|)\\
&+\eta_1^2\eta_2^2\chi^2\frac{\gamma^3+5\gamma^2\alpha_3+5\gamma\alpha_3^2+2\alpha_3^2}{\alpha_3(\gamma+\alpha_3)(\gamma+2\alpha_3)}\exp(-2\alpha_3|\tau|)+2\eta_1\eta_2\exp(-\alpha_1|\tau-\delta\tau|-\alpha_3|\tau|)\\
&\times\left\{\left[\frac{2\chi^2(\gamma+\alpha_3)}{\gamma+2\alpha_3}-\frac{\chi\chi_R\gamma_R\gamma\Delta}{\gamma(\gamma_R+\alpha_1+\alpha_3)^2+\gamma\Delta^2}-\frac{2\chi\chi_R\gamma_R\gamma\Delta}{\alpha_3(\gamma_R+\gamma+\alpha_1+\alpha_3)^2+\alpha_3\Delta^2}\right]\right.\\
&\times\cos[\Delta\vec{k}\cdot\vec{r}-(\omega_1-\omega_3)\tau+\omega_1\delta\tau]-\left[\frac{\chi\chi_R\gamma_R\gamma(\gamma_R+\alpha_1+\alpha_3)}{\gamma(\gamma_R+\alpha_1+\alpha_3)^2+\gamma\Delta^2}+\frac{2\chi\chi_R\gamma_R\gamma(\gamma+\gamma_R+\alpha_1+\alpha_3)}{\alpha_3(\gamma_R+\gamma+\alpha_1+\alpha_3)^2+\alpha_3\Delta^2}\right]\\
&\left.\times\sin\left[\Delta\vec{k}\cdot\vec{r}-(\omega_1-\omega_3)\tau+\omega_1\delta\tau\right]\right\},
\end{aligned}
\tag{22}
$$

(ii) $0<\tau<\delta\tau$

$$
\begin{aligned}
I(\Delta,\tau)\propto{}&\chi_R^2\gamma_R\left[\frac{(1+\eta_1^2+\eta_2^2)}{\alpha_1+\alpha_3}+\frac{\eta_1^2\gamma_R}{\alpha_1(\gamma_R+\alpha_3)}\right]-\frac{4\chi_R\chi\gamma_R\gamma\Delta}{\alpha_1\left[(\gamma_R+\gamma+\alpha_1+\alpha_3)^2+\Delta^2\right]}\\
&+\chi^2\gamma\left[\frac{1}{2\alpha_1}+\frac{\eta_1^2\eta_2^2(3\gamma+\alpha_3)}{2\alpha_3(\gamma+\alpha_3)}\right]+\chi^2\exp(-2\alpha_1|\tau-\delta\tau|)+\eta_1^2\eta_2^2\chi^2\frac{5\gamma+2}{2\alpha_3}\exp(-2\alpha_3|\tau|)\\
&+\frac{2\chi_R^2\gamma_R^2}{\alpha_1\alpha_3}\exp(-2\gamma_R|\tau-\delta\tau|)+2\chi^2\eta_1\eta_2\exp(-\alpha_1|\tau-\delta\tau|-\alpha_3|\tau|)\cos\left[\Delta\vec{k}\cdot\vec{r}-(\omega_1-\omega_3)\tau+\omega_1\delta\tau\right]\\
&-4\eta_1\eta_2\chi_R\chi\gamma_R\gamma\frac{\alpha_3+2\gamma}{\gamma\alpha_1\alpha_3}\exp(-\alpha_3|\tau-\delta\tau|-\alpha_3|\tau|)\sin\left[\Delta\vec{k}\cdot\vec{r}-(\omega_1-\omega_3)\tau+\omega_1\delta\tau+\Delta|\tau-\delta\tau|\right],
\end{aligned}
\tag{23}
$$

and (iii) $\tau<0$

$$
\begin{aligned}
I(\Delta,\tau)\propto{}&\chi_R^2\gamma_R\left[\frac{(1+\eta_1^2+\eta_2^2)}{\alpha_1+\alpha_3}+\frac{\eta_1^2\gamma_R}{\alpha_1(\gamma_R+\alpha_3)}\right]-\frac{4\chi_R\chi\gamma_R\gamma\Delta}{\alpha_1\left[(\gamma_R+\gamma+\alpha_1+\alpha_3)^2+\Delta^2\right]}+\chi^2\gamma\left[\frac{1}{2\alpha_1}+\frac{\eta_1^2\eta_2^2(3\gamma+\alpha_3)}{2\alpha_3(\gamma+\alpha_3)}\right]\\
&+\frac{2\chi^2\eta_1^2\eta_2^2\gamma^2}{\alpha_3^2}\exp(-2\gamma|\tau|)+\frac{2\chi_R^2\gamma_R^2}{\alpha_1\alpha_3}\left[\exp(-2\gamma_R|\tau-\delta\tau|)+\eta_2^2\exp(-2\gamma_R|\tau|)\right]\\
&+\exp(-\gamma_R|\tau-\delta\tau|-\gamma|\tau|)\frac{8\eta_1\eta_2}{\alpha_3(\alpha_1+\alpha_3)}\left\{\cos\left[\Delta\vec{k}\cdot\vec{r}-(\omega_1-\omega_3)\tau+\omega_1\delta\tau+\Delta|\tau-\delta\tau|\right]\right.\\
&\left.-\chi_R\chi\gamma_R\gamma\sin\left[\Delta\vec{k}\cdot\vec{r}-(\omega_1-\omega_3)\tau+\omega_1\delta\tau+\Delta|\tau-\delta\tau|\right]\right\}.
\end{aligned}
\tag{24}
$$

Eqs. (22)–(24) are analogous to (17)–(19), respectively. The total polarization [see Eqs. (9)–(13)], which involves the integration of t' from 0 to ∞, is the accumulation of the polarization induced at a different

time. We consider the case that the pump beams 1, 2 and 3 have a broadband linewidth so that it can be modeled as a sequence of short, phase-incoherent subpulses of duration τ_c, where τ_c is the laser coherence time [27]. Although grating can be induced by any pair of subpulses in beams 1, 2, 3 only those pairs that are phase correlated in beams 1 and 2 give rise to the τ dependence of the FWM signal. Therefore, the requirement for the existence of a τ-dependent FWM signal for $\tau > 0$ is that the phase correlated subpulses in beams 1 and 2 are overlapped temporally. Since beams 1 and 2 are mutually coherent, the temporal behavior of the REPB signal for $\tau > 0$ should coincide with the case when the pump beams are nearly monochromatic.

5. The phase-diffusion field

We have assumed that the laser sources are chaotic field in the above calculation. A chaotic field, which is used to describe a multimode laser source, is characterized by the fluctuation of both the amplitude and the phase of the field. Another commonly used stochastic model is phase-diffusion model, which is used to describe an amplitude-stabilized laser source. This model assumes that the amplitude of the laser field is a constant, while its phase fluctuates as random process. If the lasers have Lorentzian line shape, the sixth- and fourth-order coherence function is [1,5]

$$\begin{aligned}\langle u_i(t_1)u_i(t_2)u_i(t_3)u_i^*(t_4)u_i^*(t_5)u_i^*(t_6)\rangle = \exp\big[&-\alpha_i(|t_1-t_4|+|t_1-t_5|+|t_1-t_6|+|t_2-t_4|+|t_2-t_5|\\&+|t_2-t_6|+|t_3-t_4|+|t_3-t_5|+|t_3-t_6|)\big]\exp\big[\alpha_i(|t_1-t_2|\\&+|t_1-t_3|+|t_2-t_3|+|t_4-t_5|+|t_4-t_6|+|t_5-t_6|)\big],\end{aligned} \tag{25}$$

and

$$\langle u_i(t_1)u_i(t_2)u_i^*(t_3)u_i^*(t_4)\rangle = \exp\big[-\alpha_i(|t_1-t_3|+|t_1-t_4|+|t_2-t_3|+|t_2-t_4|)\big]\exp[\alpha_i(|t_1-t_2|+|t_3-t_4|)]. \tag{26}$$

We first consider the situation when the laser sources in beams 1, 2 and 3 are broadband (i.e., $\alpha_1, \alpha_3 \gg \gamma, \gamma_R$). In this limit, after substituting Eqs. (16), (25) and (26) into $I(\Delta,\tau) \propto \langle|P^{(3)}|^2\rangle$, we obtain, for:

(i) $\tau > \delta\tau$

$$\begin{aligned}I(\Delta,\tau) \propto{}& \left(1+\eta_1^2+\eta_2^2\right)\frac{\chi_R^2\gamma_R(\alpha_1+\alpha_3)}{(\alpha_1+\alpha_3)^2+\Delta^2} - \chi_R\chi\gamma_R\gamma\frac{\Delta\left[(5\alpha_1+\alpha_3)(\alpha_1+\alpha_3)+\Delta^2\right]}{2\alpha_1\left[(\alpha_1+\alpha_3)^2+\Delta^2\right]^2} + \frac{\chi^2\gamma}{2\alpha_1\alpha_3}(\alpha_1\eta_1^2\eta_2^2+\alpha_3)\\&+\left[\chi^2-\frac{2\chi\chi_R\gamma_R\Delta}{(\alpha_1+\alpha_3)^2+\Delta^2}\right]\exp(-2\alpha_1|\tau-\delta\tau|)+\eta_1^2\eta_2^2\chi^2\exp(-2\alpha_3|\tau|)\\&+2\eta_1\eta_2\exp\big(-\alpha_1|\tau-\delta\tau|-\alpha_3|\tau|\big)\left\{\left[\chi^2-\frac{\chi\chi_R\gamma_R\Delta}{(\alpha_1+\alpha_3)^2+\Delta^2}\right]\cos\left[\Delta\vec{k}\cdot\vec{r}-(\omega_1-\omega_3)\tau+\omega_1\delta\tau\right]\right.\\&\left.-\frac{\chi\chi_R\gamma_R(\alpha_1+\alpha_3)}{(\alpha_1+\alpha_3)^2+\Delta^2}\sin\left[\Delta\vec{k}\cdot\vec{r}-(\omega_1-\omega_3)\tau+\omega_1\delta\tau\right]\right\},\end{aligned} \tag{27}$$

(ii) $0 < \tau < \delta\tau/2$

$$I(\Delta,\tau) \propto \left(1+\eta_1^2+\eta_2^2\right)\frac{\chi_R^2\gamma_R(\alpha_1+\alpha_3)}{(\alpha_1+\alpha_3)^2+\Delta^2} - \chi_R\chi\gamma_R\gamma\frac{\Delta\left[(5\alpha_1+\alpha_3)(\alpha_1+\alpha_3)+\Delta^2\right]}{2\alpha_1\left[(\alpha_1+\alpha_3)^2+\Delta^2\right]^2} + \frac{\chi^2\gamma}{2\alpha_1\alpha_3}\left(\alpha_1\eta_1^2\eta_2^2+\alpha_3\right)$$
$$+\left[\chi^2 - \frac{2\chi\chi_R\gamma_R\Delta}{(\alpha_1+\alpha_3)^2+\Delta^2}\right]\exp(-2\alpha_1|\tau-\delta\tau|) + \eta_1^2\eta_2^2\chi^2\exp(-2\alpha_3|\tau|)$$
$$+2\chi^2\eta_1\eta_2\exp(-\alpha_1|\tau-\delta\tau|-\alpha_3|\tau|)\cos\left[\Delta\vec{k}\cdot\vec{r}-(\omega_1-\omega_3)\tau+\omega_1\delta\tau\right]$$
$$-2\chi\chi_R\gamma_R\gamma\eta_1\eta_2\left\{\left[\frac{2}{(\alpha_1-\alpha_3)^2+\Delta^2}+\frac{2\alpha_1}{\gamma(\alpha_1^2-\alpha_3^2)}\right]\exp(-\alpha_3|\tau-\delta\tau|-\alpha_3|\tau|)\right.$$
$$\left.+\left[\frac{1}{(\alpha_1-3\alpha_3)^2}-\frac{1}{\gamma(\alpha_1-\alpha_3)}\right]\exp(-\alpha_1|\tau-\delta\tau|-\alpha_3|\tau|)\right\}\sin\left[\Delta\vec{k}\cdot\vec{r}-(\omega_1-\omega_3)\tau+\omega_1\delta\tau\right], \tag{28}$$

(iii) $\delta\tau/2 < \tau < \delta\tau$

$$I(\Delta,\tau) \propto \left(1+\eta_1^2+\eta_2^2\right)\frac{\chi_R^2\gamma_R(\alpha_1+\alpha_3)}{(\alpha_1+\alpha_3)^2+\Delta^2} - \chi_R\chi\gamma_R\gamma\frac{\Delta\left[(5\alpha_1+\alpha_3)(\alpha_1+\alpha_3)+\Delta^2\right]}{2\alpha_1\left[(\alpha_1+\alpha_3)^2+\Delta^2\right]^2} + \frac{\chi^2\gamma}{2\alpha_1\alpha_3}\left(\alpha_1\eta_1^2\eta_2^2+\alpha_3\right)$$
$$+\left[\chi^2 - \frac{2\chi\chi_R\gamma_R\Delta}{(\alpha_1+\alpha_3)^2+\Delta^2}\right]\exp(-2\alpha_1|\tau-\delta\tau|) + \eta_1^2\eta_2^2\chi^2\exp(-2\alpha_3|\tau|)$$
$$+2\chi^2\eta_1\eta_2\exp(-\alpha_1|\tau-\delta\tau|-\alpha_3|\tau|)\cos[\Delta\vec{k}\cdot\vec{r}-(\omega_1-\omega_3)\tau+\omega_1\delta\tau] - 2\chi\chi_R\gamma_R\gamma\eta_1\eta_2$$
$$\times\left[\frac{2\alpha_1}{\gamma(\alpha_1^2-\alpha_3^2)}\exp(-\alpha_3|\tau-\delta\tau|-\alpha_3|\tau|) - \frac{1}{\gamma(\alpha_1-\alpha_3)^2+\gamma\Delta^2}\exp(-\alpha_1|\tau-\delta\tau|-\alpha_3|\tau|)\right]$$
$$\times\sin\left[\Delta\vec{k}\cdot\vec{r}-(\omega_1-\omega_3)\tau+\omega_1\delta\tau\right], \tag{29}$$

(iv) $\tau < 0$ and $\alpha_1|\tau|, \alpha_3|\tau| \gg 1$

$$I(\Delta,\tau) \propto \left(1+\eta_1^2+\eta_2^2\right)\frac{\chi_R^2\gamma_R(\alpha_1+\alpha_3)}{(\alpha_1+\alpha_3)^2+\Delta^2} - \chi_R\chi\gamma_R\gamma\frac{\Delta\left[(5\alpha_1+\alpha_3)(\alpha_1+\alpha_3)+\Delta^2\right]}{2\alpha_1\left[(\alpha_1+\alpha_3)^2+\Delta^2\right]^2}$$
$$+\frac{\chi^2\gamma}{2\alpha_1\alpha_3}\left(\alpha_1\eta_1^2\eta_2^2+\alpha_3\right) - \exp[-\alpha_1|\delta\tau|-(\gamma_R+\gamma)|\tau|]\frac{4\eta_1\eta_2\chi\chi_R\gamma\gamma_R\left[(\alpha_1+2\alpha_3)(\alpha_1+\alpha_3)^2+\alpha_1\Delta^2\right]}{\alpha_3\left[(\alpha_1+\alpha_3)^2+\Delta^2\right]}$$
$$\times\sin\left[\Delta\vec{k}\cdot\vec{r}-(\omega_1-\omega_3)\tau+\omega_1\delta\tau+\Delta|\tau-\delta\tau|\right]. \tag{30}$$

Eqs. (27)–(29) indicate that when $\tau > 0$, the temporal behavior of the beat signal intensity reflects mainly the characteristic of the lasers. When $\tau < 0$, Eq. (30) is mainly determined by a molecule vibrational property.

We then consider the situation when the laser sources in beams 1, 2 and 3 are narrow band (i.e., $\alpha_1, \alpha_3 \ll \gamma, \gamma_R$ and $\gamma_R|\tau|, \gamma|\tau| \gg 1$). In this limit, after performing the tedious integration we obtain

$$I(\Delta,\tau) \propto \left(1+\eta_1^2+\eta_2^2\right)\frac{\chi_R^2\gamma_R^2}{\gamma_R^2+\Delta^2} - \frac{\chi_R\chi\gamma_R\Delta}{\gamma_R^2+\Delta^2} + \chi^2\left(1+\eta_1^2\eta_2^2\right) + 2\eta_1\eta_2\exp(-\alpha_1|\tau-\delta\tau| - \alpha_3|\tau|)$$
$$\times\left\{\left(\chi^2 - \frac{\chi\chi_R\gamma_R\Delta}{\gamma_R^2+\Delta^2}\right)\cos\left[\Delta\vec{k}\cdot\vec{r} - (\omega_1-\omega_3)\tau + \omega_1\delta\tau\right]\right.$$
$$\left. - \frac{\chi\chi_R\gamma_R^2}{\gamma_R^2+\Delta^2}\sin\left[\Delta\vec{k}\cdot\vec{r} - (\omega_1-\omega_3)\tau + \omega_1\delta\tau\right]\right\}. \tag{31}$$

Eq. (31) indicates that the temporal behavior of the beat signal intensity reflects mainly the characteristic of the lasers.

After that, based on phase-diffusion model, we consider the three-pulse Raman echo when the laser sources have a broadband linewidth. Substituting Eqs. (16), (21), (25) and (26) into $I(\Delta,\tau) \propto \langle|P^{(3)}|^2\rangle$, we obtain, for:

(i) $\tau > 0$

$$I(\Delta,\tau) \propto \left(1+\eta_1^2+\eta_2^2\right)\frac{\chi_R^2\gamma_R}{\alpha_1+\alpha_3} - \frac{4\chi_R\chi\gamma_R\gamma\Delta}{\alpha_1\left[(\gamma_R+\gamma+\alpha_1+\alpha_3)^2+\Delta^2\right]} + \frac{\chi^2\gamma}{2\alpha_1\alpha_3}\left(\alpha_1\eta_1^2\eta_2^2+\alpha_3\right)$$
$$+ 2\eta_1\eta_2\chi^2\exp(-\alpha_1|\tau-\delta\tau| - \alpha_3|\tau|)\cos\left[\Delta\vec{k}\cdot\vec{r} - (\omega_1-\omega_3)\tau + \omega_1\delta\tau\right], \tag{32}$$

and (ii) $\tau < 0$

$$I(\Delta,\tau) \propto \left(1+\eta_1^2+\eta_2^2\right)\frac{\chi_R^2\gamma_R}{\alpha_1+\alpha_3} - \frac{4\chi_R\chi\gamma_R\gamma\Delta}{\alpha_1\left[(\gamma_R+\gamma+\alpha_1+\alpha_3)^2+\Delta^2\right]} + \frac{\chi^2\gamma}{2\alpha_1\alpha_3}\left(\alpha_1\eta_1^2\eta_2^2+\alpha_3\right)$$
$$+ 2\eta_1\eta_2\chi^2\exp(-\alpha_1|\tau-\delta\tau| - \alpha_3|\tau|)\cos\left[\Delta\vec{k}\cdot\vec{r} - (\omega_1-\omega_3)\tau + \omega_1\delta\tau\right] - \exp[-\alpha_1|\delta\tau|$$
$$- (\gamma_R+\gamma)|\tau|]\frac{8\eta_1\eta_2\chi\chi_R\gamma\gamma_R}{\alpha_3^2}\sin\left[\Delta\vec{k}\cdot\vec{r} - (\omega_1-\omega_3)\tau + \omega_1\delta\tau + \Delta|\tau-\delta\tau|\right]. \tag{33}$$

Eqs. (32) and (33) are analogous to Eqs. (31) and (30), respectively.

Eqs. (27)–(33) are different from the result based on a chaotic model. Relation (27) consists of six terms. The sixth term depending on the $u_1(t)$ or $u_3(t)$ fourth- and second-order coherence functions is the cross-correlation intensity between five third-order nonlinear polarizations, and gives rise to the modulation of the beat signal. The other terms (the τ-independent terms and the decay terms) depending on the sixth-, fourth- or second-order coherence functions of $u_1(t)$ or $u_3(t)$ are a sum of the auto-correlation intensity between five third-order nonlinear polarizations. Different stochastic models of the laser field affect only the sixth- and fourth-order coherence functions. Eqs. (30) and (33) are short of the decay terms including these factors $\exp(-2\gamma|\tau|)$ and $\exp(-2\gamma_R|\tau|)$. Eqs. (31) and (32) are also short of the decay terms including these factors $\exp(-2\alpha_1|\tau|)$ and $\exp(-2\alpha_3|\tau|)$. These are shown to be particularly insensitive to the phase fluctuation of the Markovian stochastic light fields [6–10]. The drastic difference of the results also exists in the fourth-order coherence on ultrafast modulation spectroscopy when these two models are employed [6]. Physically, the chaotic field has the property of photon bunching, which can affect any multiphoton process when the higher-order correlation function of the field plays an important role.

6. The Gaussian-amplitude field

The Gaussian-amplitude field has a constant phase but its real amplitude undergoes Gaussian fluctuations. If the lasers have Lorentzian line shape, the sixth- and fourth-order coherence function is [1,5]

$$\begin{aligned}
&\langle u_i(t_1)u_i(t_2)u_i(t_3)u_i(t_4)u_i(t_5)u_i(t_6)\rangle \\
&\quad = \langle u_i(t_1)u_i(t_4)\rangle\langle u_i(t_2)u_i(t_3)u_i(t_5)u_i(t_6)\rangle + \langle u_i(t_1)u_i(t_5)\rangle\langle u_i(t_2)u_i(t_3)u_i(t_4)u_i(t_6)\rangle \\
&\qquad + \langle u_i(t_1)u_i(t_6)\rangle\langle u_i(t_2)u_i(t_3)u_i(t_4)u_i(t_5)\rangle + \langle u_i(t_1)u_i(t_2)\rangle\langle u_i(t_3)u_i(t_4)u_i(t_5)u_i(t_6)\rangle \\
&\qquad + \langle u_i(t_1)u_i(t_3)\rangle\langle u_i(t_2)u_i(t_4)u_i(t_5)u_i(t_6)\rangle
\end{aligned} \tag{34}$$

and

$$\begin{aligned}
\langle u_i(t_1)u_i(t_2)u_i(t_3)u_i(t_4)\rangle &= \langle u_i(t_1)u_i(t_3)\rangle\langle u_i(t_2)u_i(t_4)\rangle + \langle u_i(t_1)u_i(t_4)\rangle\langle u_i(t_2)u_i(t_3)\rangle \\
&\quad + \langle u_i(t_1)u_i(t_2)\rangle\langle u_i(t_3)u_i(t_4)\rangle.
\end{aligned} \tag{35}$$

Based on the Gaussian-amplitude field, we first consider the case when the laser sources have a broadband linewidth. Substituting Eqs. (16), (34) and (35) into $I(\Delta,\tau)\propto\langle|P^{(3)}|^2\rangle$, we obtain as follows:

(i) $\tau > \delta\tau$

$$\begin{aligned}
I(\Delta,\tau) \propto{}& \chi_R^2\gamma_R\frac{(\alpha_1+\alpha_3)\left(1+\eta_1^2+\eta_2^2\right)}{(\alpha_1+\alpha_3)^2+\Delta^2} + \chi^2\gamma\left[\frac{\eta_1^2\eta_2^2(1+\alpha_3)}{2\alpha_3^2}+\frac{1}{2\alpha_1}\right] \\
&+\left\{\frac{2\chi_R^2\gamma_R^2(\alpha_1+\alpha_3)}{\alpha_1\left[(\alpha_1+\alpha_3)^2+\Delta^2\right]}+\chi^2-\frac{2\chi_R\chi\gamma_R\Delta}{(\alpha_1+\alpha_3)^2+\Delta^2}\right\}\exp(-2\alpha_1|\tau-\delta\tau|) \\
&+\left\{\frac{2\chi_R^2\gamma_R^2\eta_2^2(\alpha_1+\alpha_3)}{\alpha_3\left[(\alpha_1+\alpha_3)^2+\Delta^2\right]}+\eta_1^2\chi^2+\frac{\eta_1^2\eta_2^2\chi^2\gamma}{2\alpha_3^2}\right\}\exp(-2\alpha_3|\tau|)+2\eta_1\eta_2\exp(-\alpha_1|\tau-\delta\tau|-\alpha_3|\tau|) \\
&\times\left\{\left[\frac{\chi^2\gamma}{2\alpha_3}+\chi^2-\frac{\chi_R\chi\gamma_R\Delta}{(\alpha_1+\alpha_3)^2+\Delta^2}\left(1+\frac{\gamma}{2\alpha_3}\right)\right]\cos\left[\Delta\vec{k}\cdot\vec{r}-(\omega_1-\omega_3)\tau+\omega_1\delta\tau\right]\right. \\
&\left.-\frac{\chi_R\chi\gamma_R(\alpha_1+\alpha_3)}{(\alpha_1+\alpha_3)^2+\Delta^2}\left(2+\frac{\gamma}{2\alpha_3}\right)\sin\left[\Delta\vec{k}\cdot\vec{r}-(\omega_1-\omega_3)\tau+\omega_1\delta\tau\right]\right\} \\
&-\frac{4\eta_1\eta_2\chi\chi_R\gamma_R\gamma\alpha_3}{(\alpha_1+\alpha_3)(\alpha_1^2-\alpha_3^2)}\exp(-2\alpha_1|\tau-\delta\tau|)\sin\left[\Delta\vec{k}\cdot\vec{r}-(\omega_1-\omega_3)\tau+\omega_1\delta\tau+\Delta|\tau-\delta\tau|\right],
\end{aligned} \tag{36}$$

(ii) $0 < \tau < \delta\tau/2$

$$\begin{aligned}
I(\Delta,\tau) \propto{}& \chi_R^2\gamma_R\frac{(\alpha_1+\alpha_3)\left(1+\eta_1^2+\eta_2^2\right)}{(\alpha_1+\alpha_3)^2+\Delta^2} + \chi^2\gamma\left[\frac{\eta_1^2\eta_2^2(1+\alpha_3)}{2\alpha_3^2}+\frac{1}{2\alpha_1}\right] \\
&+\left\{\frac{\chi_R^2\gamma_R^2(\alpha_1+\alpha_3)}{\alpha_1\left[(\alpha_3-\alpha_1)^2+\Delta^2\right]}+\chi^2\right\}\exp(-2\alpha_1|\tau-\delta\tau|)
\end{aligned}$$

$$+\left\{\frac{\chi_R^2\gamma_R^2\eta_2^2(\alpha_1+\alpha_3)}{\alpha_1\left[(\alpha_1-\alpha_3)^2+\Delta^2\right]}+\chi^2+\frac{\eta_1^2\eta_2^2\chi^2\gamma}{2\alpha_3}\right\}\exp(-2\alpha_3|\tau|)$$

$$+\exp(-2\gamma_R|\tau-\delta\tau|)\left\{\frac{\chi_R^2\gamma_R^2}{\alpha_1(\alpha_1+\alpha_3)}+\frac{2\chi_R^2\gamma_R^2[\alpha_1+\alpha_3-(\alpha_1+\alpha_3)^2+\Delta^2]}{\alpha_1\left[(\alpha_1+\alpha_3)^2+\Delta^2\right]}\right\}$$

$$+\eta_1\eta_2\left(\frac{\chi^2}{2}+\frac{\chi\chi_R\gamma}{2\alpha_3}\right)\exp(-\alpha_1|\tau-\delta\tau|-\alpha_3|\tau|)\cos\left[\Delta\vec{k}\cdot\vec{r}-(\omega_1-\omega_3)\tau+\omega_1\delta\tau\right]$$

$$+\eta_1\eta_2\chi_R\chi\gamma_R\gamma\left[\frac{1}{\gamma(\alpha_1+\alpha_3)}\exp(-\alpha_1|\tau-\delta\tau|-\alpha_3|\tau|)+\frac{2\alpha_1}{\gamma(\alpha_1^2-\alpha_3^2)}\exp(-\alpha_3|\tau-\delta\tau|-\alpha_3|\tau|)\right]$$

$$\times\sin\left[\Delta\vec{k}\cdot\vec{r}-(\omega_1-\omega_3)\tau+\omega_1\delta\tau+\Delta|\tau-\delta\tau|\right], \tag{37}$$

(iii) $\delta\tau/2<\tau<\delta\tau$

$$I(\Delta,\tau)\propto\chi_R^2\gamma_R\frac{(\alpha_1+\alpha_3)(1+\eta_1^2+\eta_2^2)}{(\alpha_1+\alpha_3)^2+\Delta^2}+\chi^2\gamma\left[\frac{\eta_1^2\eta_2^2(1+\alpha_3)}{2\alpha_3^2}+\frac{1}{2\alpha_1}\right]+\left\{\frac{\chi_R^2\gamma_R^2(\alpha_1+\alpha_3)}{\alpha_1\left[(\alpha_3-\alpha_1)^2+\Delta^2\right]}+\chi^2\right\}$$

$$\times\exp(-2\alpha_1|\tau-\delta\tau|)+\left\{\frac{\chi_R^2\gamma_R^2\eta_2^2(\alpha_1+\alpha_3)}{\alpha_1\left[(\alpha_1-\alpha_3)^2+\Delta^2\right]}+\chi^2+\frac{\eta_1^2\eta_2^2\chi^2\gamma}{2\alpha_3}\right\}\exp(-2\alpha_3|\tau|)$$

$$+\exp(-2\gamma_R|\tau-\delta\tau|)\left\{\frac{\chi_R^2\gamma_R^2}{\alpha_1(\alpha_1+\alpha_3)}+\frac{2\chi_R^2\gamma_R^2\left[\alpha_1+\alpha_3-(\alpha_1+\alpha_3)^2+\Delta^2\right]}{\alpha_1\left[(\alpha_1+\alpha_3)^2+\Delta^2\right]}\right\}$$

$$+\eta_1\eta_2\left(\frac{\chi^2}{2}+\frac{\chi\chi_R\gamma}{2\alpha_3}\right)\exp(-\alpha_1|\tau-\delta\tau|-\alpha_3|\tau|)\cos\left[\Delta\vec{k}\cdot\vec{r}-(\omega_1-\omega_3)\tau+\omega_1\delta\tau\right]$$

$$+\eta_1\eta_2\chi_R\chi\gamma_R\gamma\left[\frac{1}{\gamma(\alpha_1+\alpha_3)}\exp(-\alpha_1|\tau-\delta\tau|-\alpha_3|\tau|)+\frac{1}{2\alpha_3(\alpha_1+\alpha_3)}\exp(-\alpha_3|\tau-\delta\tau|-\alpha_3|\tau|)\right]$$

$$\times\sin\left[\Delta\vec{k}\cdot\vec{r}-(\omega_1-\omega_3)\tau+\omega_1\delta\tau+\Delta|\tau-\delta\tau|\right], \tag{38}$$

and (iv) $\tau<0$ and $\alpha_1|\tau|,\alpha_3|\tau|\gg1$

$$I(\Delta,\tau)\propto\chi_R^2\gamma_R\frac{(\alpha_1+\alpha_3)(1+\eta_1^2+\eta_2^2)}{(\alpha_1+\alpha_3)^2+\Delta^2}+\chi^2\gamma\left[\frac{\eta_1^2\eta_2^2(1+\alpha_3)}{2\alpha_3^2}+\frac{1}{2\alpha_1}\right]$$

$$+\frac{3\chi^2\eta_1^2\eta_2^2\gamma^2}{2\alpha_3^2}\exp(-2\gamma|\tau|)+\frac{\chi_R^2\gamma_R^2}{(\alpha_1+\alpha_3)^2+\Delta^2}\left\{\left[\alpha_3+(\alpha_1+\alpha_3)^2-\Delta^2+\frac{2\alpha_3}{\alpha_1}\right]\exp(-2\gamma_R|\tau|)\right.$$

$$\left.+\eta_2^2\left[\alpha_1+(\alpha_1+\alpha_3)^2-\Delta^2+\frac{2\alpha_1}{\alpha_3}\right]\exp(-2\gamma_R|\tau-\delta\tau|)\right\}+\exp(-\gamma_R|\tau-\delta\tau|-\gamma|\tau|)$$

$$\times\frac{4\chi_R\chi\gamma_R\gamma\eta_1\eta_2}{\alpha_3\left[(\alpha_1+\alpha_3)^2+\Delta^2\right]}\left\{(\alpha_1+\alpha_3)(2\gamma_R+\gamma)\Delta\cos\left[\Delta\vec{k}\cdot\vec{r}-(\omega_1-\omega_3)\tau+\omega_1\delta\tau\right]\right.$$

$$\left.-\left[(\alpha_1+2\alpha_3)(\alpha_1+\alpha_3)^2+\alpha_1\Delta^2\right]\sin\left[\Delta\vec{k}\cdot\vec{r}-(\omega_1-\omega_3)\tau+\omega_1\delta\tau+\Delta|\tau-\delta\tau|\right]\right\}. \tag{39}$$

Eq. (36) indicates that when $\tau > \delta\tau$, the temporal behavior of the beat signal intensity reflects mainly the characteristic of the lasers. When $0 < \tau < \delta\tau/2$ and $\delta\tau/2 < \tau < \delta\tau$, Eqs. (37) and (38) reflect not only the characteristic of the lasers, but also a material vibrational property. When $\tau < 0$, Eq. (39) is mainly determined by a material vibrational property.

We then consider the situation when the laser sources in beams 1, 2 and 3 are narrow band (i.e., $\alpha_1, \alpha_3 \ll \gamma, \gamma_R$ and $\gamma_R|\tau|, \gamma|\tau| \gg 1$). In this limit, after performing the tedious integration we obtain

$$
\begin{aligned}
I(\Delta,\tau) \propto{}& \frac{\chi_R^2\gamma_R^2\left(1+3\eta_1^2+\eta_2^2\right)}{\gamma_R^2+\Delta^2}+\chi^2\left(1+3\eta_1^2\eta_2^2\right)-\frac{2\chi\chi_R\gamma_R\Delta}{\gamma_R^2+\Delta^2}+2\left(\frac{\chi_R^2\gamma_R^2}{\gamma_R^2+\Delta^2}+\chi^2-\frac{\chi\chi_R\gamma_R\Delta}{\gamma_R^2+\Delta^2}+\chi\chi_R\right)\\
&\times\exp(-2\alpha_1|\tau-\delta\tau|)+2\left(\frac{\chi_R^2\gamma_R^2\eta_2^2}{\gamma_R^2+\Delta^2}+6\chi^2\eta_1^2\eta_2^2\right)\exp(-2\alpha_3|\tau|)+2\eta_1\eta_2\exp(-\alpha_1|\tau-\delta\tau|-\alpha_3|\tau|)\\
&\times\left\{\left[\frac{2\chi\chi_R\gamma_R\Delta\alpha_3}{\gamma(\gamma_R+\gamma)^2+\gamma\Delta^2}-\frac{2\chi\chi_R\gamma_R\Delta}{\gamma_R^2+\Delta^2}+3\chi^2\right]\cos\left[\Delta\vec{k}\cdot\vec{r}-(\omega_1-\omega_3)\tau+\omega_1\delta\tau\right]\right.\\
&\left.+\chi_R\chi\gamma_R\left[\frac{2\alpha_3(\gamma+\gamma_R)}{\gamma(\gamma_R+\gamma)^2+\gamma\Delta^2}+\frac{1}{\gamma}-\frac{2\gamma_R}{\gamma_R^2+\Delta^2}\right]\sin\left[\Delta\vec{k}\cdot\vec{r}-(\omega_1-\omega_3)\tau+\omega_1\delta\tau\right]\right\}. \qquad (40)
\end{aligned}
$$

Eq. (40) is analogous to (36), which indicates that the temporal behavior of the beat signal intensity reflects mainly the characteristic of the lasers.

Relation (36) consists of six terms. The fifth and sixth terms depending on the $u_1(t)$ or $u_3(t)$ fourth- and second-order coherence functions are the cross-correlation intensity between five third-order nonlinear polarizations, and gives rise to the modulation of the beat signal. The interferometric contrast ratio mainly determined the modulation term is equally sensitive to the amplitude and phase fluctuations of the Markovian stochastic light fields. The other term depending on the sixth-, fourth- or second-order coherence functions of $u_1(t)$ or $u_3(t)$ is a sum of the auto-correlation intensity between five third-order nonlinear polarizations. Different stochastic models of the laser field affect only the sixth- and fourth-order coherence functions. The constant terms in relations (36)–(40), which are independent of the relative time-delay between beams 1 and 2, mainly originate from the amplitude fluctuation of the Gaussian-amplitude field. The third and fourth terms in relation (36), which are shown to be particularly sensitive to the amplitude fluctuation of the Gaussian-amplitude field, indicate an exponential decay of the beat signal as $|\tau|$ increases. The τ-independent terms of Eq. (36) is identical to those of Eqs. (37)–(39). Physically, when $|\tau| \to \infty$, beams 1 and 2 are mutually incoherent, therefore whether τ is positive or negative does not affect the REPB. Eqs. (36)–(40) also indicate that beat signal oscillates not only temporally but also spatially along the direction $\Delta\vec{k}$, which is almost perpendicular to the propagation direction of the beat signal. Three three-dimensional plots of the beat signal intensity $I(\tau,\Delta)$ versus time delay τ and frequency detuning Δ, $I(\tau,r)$ versus time delay τ and transverse distance r and $I(\Delta,r)$ versus frequency detuning Δ and transverse distance r, respectively, have larger constant background caused by the intensity fluctuation of the Gaussian-amplitude field in Figs. 4(a)–(c). At zero relative time delay ($\tau = 0$ and $\delta\tau = 0$), the twin beams originating from the same source enjoy perfect overlap at the sample of their corresponding noise patterns in Figs. 4(a) and (b). This gives maximum interferometric contrast. As $|\tau|$ is increased, the interferometric contrast diminishes on the time scale that reflects material memory, usually much longer than the correlation time of the light. As $\delta\tau$ is increased, the contrast ratio is seen to diminish and the symmetry of the interferogram is destroyed in Figs. 4(a) and (b).

It is important to note that these three types of fields can have the same spectral density and thus the same second-order coherence function. The fundamental differences in the statistics of these fields are

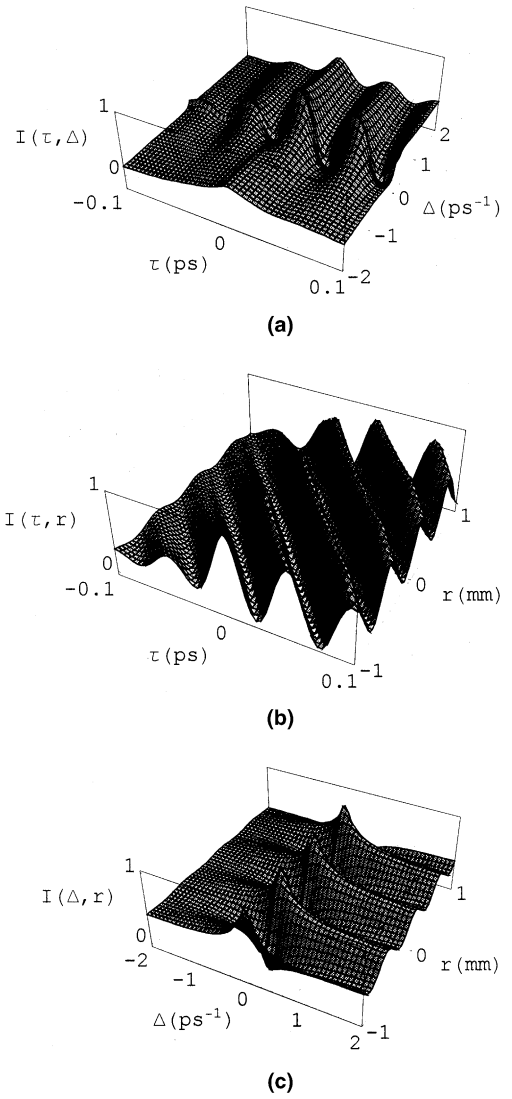

Fig. 4. Three three-dimensional plots of the beat signal intensity $I(\tau, \Delta)$ versus time delay τ and frequency detuning Δ, $I(\tau, r)$ versus time delay τ and transverse distance r and $I(\Delta, r)$ versus frequency detuning Δ and transverse distance r, respectively. The parameters are $\omega_1 = 3200\ \text{ps}^{-1}$, $\omega_3 = 3324\ \text{ps}^{-1}$, $\delta\tau = 83$ fs, $\alpha_1 = 10.8\ \text{ps}^{-1}$, $\alpha_3 = 11.6\ \text{ps}^{-1}$, $\theta = 2.62 \times 10^{-2}$ rad, $\chi/\chi_R = 1$, $\gamma_R = 0.05\ \text{ps}^{-1}$, $\gamma = 0.2\ \text{ps}^{-1}$, $\eta_1 = \eta_2 = 1$; while $\Delta k = 0\ \text{mm}^{-1}$ for (a), $\Delta k = 10.83\ \text{mm}^{-1}$, $\Delta = 0$ for (b) and $\Delta k = 10.83\ \text{mm}^{-1}$, $\tau = 0$ ps for (c).

manifest only in the higher-order coherence functions [1–10]. The term "higher order" refers to all orders larger than the second. In this paper, different stochastic models of the laser field only affect the sixth- and fourth-order coherence functions. Figs. 5(a) and (b) present the beat signal intensity versus relative time delay using laser linewidths 1 and 4 nm, respectively. The three curves in the figures represent the chaotic field (dotted line), phase-diffusion field (dashed line), and Gaussian-amplitude field (solid line), respectively. For beat pattern concision, the same constant intensity was subtracted from three signals. (Here we only interested the relative compare value in three of them. The intensity goes negative for some calculations.

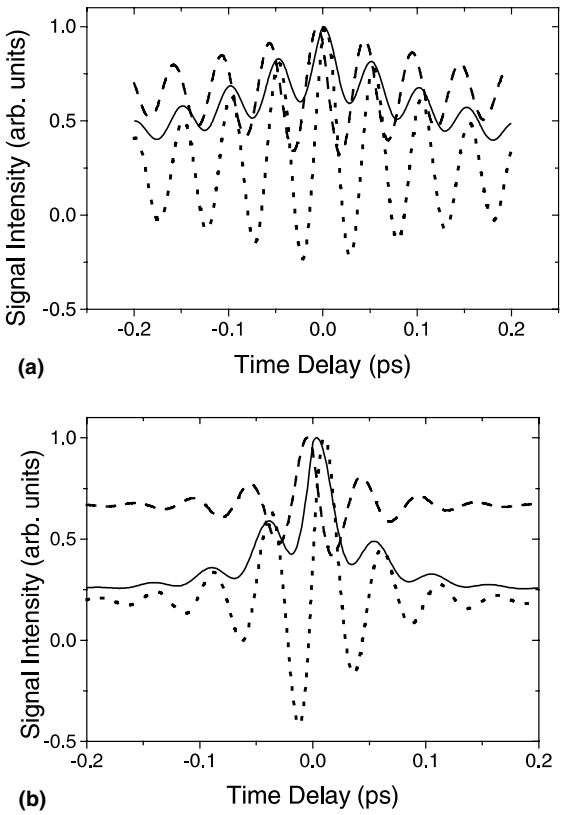

Fig. 5. The beat signal intensity versus relative time delay. The three curves represent the chaotic field (dotted line), phase-diffusion field (dashed line), and Gaussian-amplitude field (solid line). The parameters are $\omega_1 = 3200$ ps^{-1}, $\omega_3 = 3324$ ps^{-1}, $\Delta k = 0$, $\delta\tau = 0$ fs, $\eta_1 = \eta_2 = 1$, $\Delta = 0$, $\chi/\chi_R = 1$, $\gamma_R = 0.05$ ps^{-1}, $\gamma = 0.2$ ps^{-1}; while $\alpha_1 = 2.7$ ps^{-1}, $\alpha_3 = 2.9$ ps^{-1} for (a) and $\alpha_1 = 10.8$ ps^{-1}, $\alpha_3 = 11.6$ ps^{-1} for (b).

Actually that cannot happen to the total intensity.) The peak-to-background contrast ratio of the chaotic field is much larger than that of the phase-diffusion field or the Gaussian-amplitude field. Furthermore, the contrast ratio of the phase-diffusion field is slightly larger than that of the Gaussian-amplitude field. The physical explanation for this is that the signal contrast ratio is equally sensitive to the amplitude and phase fluctuations of the Markovian stochastic fields.The polarization beat signal is shown to be particularly sensitive to the statistical properties of the Markovian stochastic light fields with arbitrary bandwidth. This is quite different from the fourth-order partial-coherence effects in the formation of integrated-intensity gratings with pulsed light sources [31]. Their results proved to be insensitive to the specific radiation models. Figs. 6(a) and (b) show the interferogram of the beat signal intensity versus time delay and the spectrum of the beat signal intensity versus frequency detuning. The constant background of the beat signal for a Gaussian-amplitude field or a chaotic field is much larger than that of the signal for a phase-diffusion field in Figs. 6(a) and (b). The physical explanation for this is that the Gaussian-amplitude field undergoes stronger intensity fluctuations than a chaotic field. On the other hand, the intensity (amplitude) fluctuations of the Gaussian-amplitude field or the chaotic field are always much larger than the pure phase fluctuations of the phase-diffusion field.

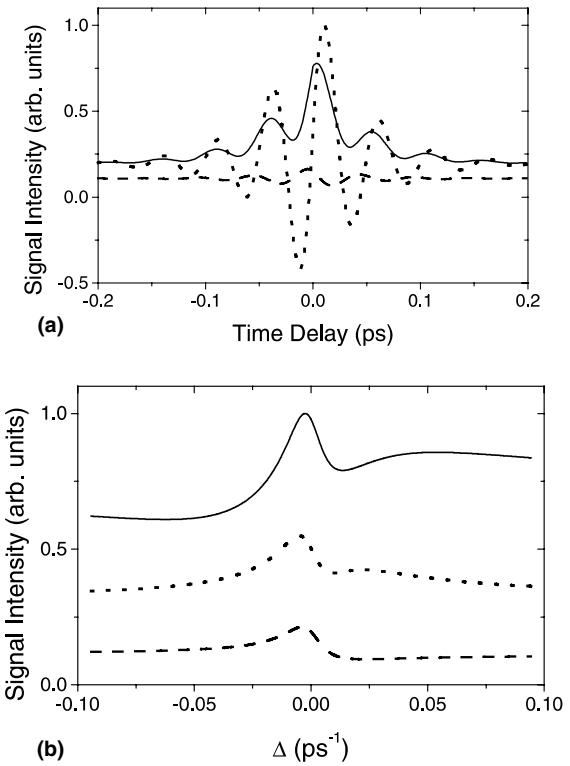

Fig. 6. The interferogram of the beat signal intensity versus time delay and the spectrum of the beat signal intensity versus frequency detuning. The three curves represent the chaotic field (dotted line), phase-diffusion field (dashed line), and Gaussian-amplitude field (solid line). The parameters are $\omega_1 = 3200\ \text{ps}^{-1}$, $\omega_3 = 3324\ \text{ps}^{-1}$, $\Delta k = 0$, $\delta\tau = 0$ fs, $\eta_1 = \eta_2 = 1$, $\chi/\chi_R = 1$, $\gamma_R = 0.05\ \text{ps}^{-1}$, $\gamma = 0.2\ \text{ps}^{-1}$; while $\Delta = 0$, $\alpha_1 = 10.8\ \text{ps}^{-1}$, $\alpha_3 = 11.6\ \text{ps}^{-1}$ for (a) and $\tau = 0$ fs, $\alpha_1 = 2.7\ \text{ps}^{-1}$, $\alpha_3 = 2.9\ \text{ps}^{-1}$ for (b).

Now, we discuss the difference between REPB and UMS with self-diffraction geometry from a physical viewpoint. The frequency and wave vector of the UMS are $\omega_{s_1} = 2\omega_1 - \omega_1$, $\omega_{s_2} = 2\omega_2 - \omega_2$ and $\vec{k}_{s_1} = 2\vec{k}_1' - \vec{k}_1$, $\vec{k}_{s_2} = 2\vec{k}_2' - \vec{k}_2$, respectively, which means that a photon is absorbed from each of the two mutually correlated pump beams. On the other hand, the frequency and wave vector of the FWM signal of the REPB are $\omega_{s_1} = \omega_1 - \omega_1 + \omega_3$, $\omega_{s_2} = \omega_3 - \omega_3 + \omega_3$, and, $\vec{k}_{s_1} = \vec{k}_1 - \vec{k}_1' + \vec{k}_3$, $\vec{k}_{s_2} = \vec{k}_2 - \vec{k}_2' + \vec{k}_3$, respectively, therefore photons are absorbed from and emitted to the mutually correlated beams 1 and 2, respectively. This difference between the REPB and UMS has profound influence on the field-correlation effects. We note that the roles of two composite beams are interchangeable in the UMS, this interchangeable feature also makes the second-order coherence function theory failure in the UMS. In virtue of $\langle u(t_1)u(t_2)\rangle = 0$, the absolute square of the stochastic average of the polarization $|\langle P^{(3)}\rangle|^2$ cannot be used to describe the temporal behavior of the UMS [17–22]. Our higher-order theory is of vital importance in the UMS [6–10].

The main purpose of the above discussion is that we reveal an important fact that the amplitude and phase fluctuations play a critical role in the temporal behavior of REPB signal. Furthermore, the different roles of the phase fluctuation and amplitude fluctuation have been pointed out in the time domain and frequency domain. This is quite different from the time delayed FWM with incoherent light in a two-level system [27]. For the latter case, the phase fluctuation of the light field is crucial. But the amplitude and

phase fluctuations of the Markovian stochastic light fields are equally crucial in the REPB. On the other hand, because of $\langle u_i(t)\rangle = 0$ and $\langle u_i^*(t)\rangle = 0$, the absolute square of the stochastic average of the polarization $|\langle P^{(3)}\rangle|^2$, which involves second-order coherence function of $u_i(t)$, cannot be used to describe the temporal behavior of the REPB. The sixth-order theory reduces to the second-order theory in the case that the laser pulse width is much longer than the laser coherence time [31]. The second-order coherence function theory is valid when we are only interested in the τ-dependent part of the beating signal [17–22]. Therefore, the sixth-order coherence function theory is of vital importance in REPB. The application of these results to the REPB experiment yielded a better fit to the data than an expression involving only second-order coherence [6–10,31]. In this paper, we present experimental results for the material response in REPB with phase-conjugation geometry using broadband chaotic fields. At present, it is difficult to achieve the polarization beat experiment by the phase-diffusion field or the Gaussian-amplitude field. Therefore, it is more difficult to get a clear picture of physical origins of the effects in each type of fluctuating field in the experiment.

7. Experiment and result

We are interested in the temporal behavior of the REPB signal intensity with fixed frequency detuning. The carbon disulfide (CS_2) with 655.7-cm^{-1} vibrational mode was contained in a sample cell with thickness 9 mm. The second harmonic of a Quanta-Ray YAG laser was used to pump two dye lasers (DL1 and DL2). Broadband sources DL1 and DL2 had linewidth 1 nm, pulse width 10 ns and output energy 1 mJ. The first dye laser DL1 had wavelength 589 nm. The wavelength of DL2 was approximately 567 nm and could be scanned by a computer-controlled stepping motor. A beam splitter was used to combine the central frequencies ω_1 and ω_3 components derived from broadband sources DL1 and DL2, respectively, for beams 1 and 2, which intersected in the sample with a small angle $\theta = 1.5°$. The relative time delay τ between beams 1 and 2 could be varied. Beam 3, which propagated along the direction opposite to that of beam 1, was also derived from broadband source DL2. All the incident beams were linearly polarized in the same direction. The beat signal had the same polarization as the incident beams, propagated along a direction almost opposite to that of beam 2. It was detected by a photodiode.

We first performed a nondegenerate FWM experiment in which beams 1 and 2 only consisted of ω_1 frequency component. We measured the RENFWM spectrum with fixed time delay by scanning ω_3. Our results are showed in Fig. 7, which showed an asymmetrical resonant profile due to the interference between the Raman resonant term and the nonresonant background originating solely from the molecular reorientational grating [23–26]. From this spectrum ω_3 was tuned to the resonant frequency (i.e., $\Delta = |\omega_1 - \omega_3| - \Omega_R = 0$). We then performed the REPB experiment with fixed frequency detuning by measuring the beat signal intensity as a function of the relative time delay when beams 1 and 2 consist of both frequencies ω_1 and ω_3. Fig. 8 presents the result of the polarization beat experiment. The beat signal intensity modulates sinusoidally with period 51 fs. The modulation frequency can be obtained more directly by making a Fourier transformation of the REPB data. Fig. 9 shows the Fourier spectrum of the REPB data in which τ is varied for a range of 5 ps. Then we obtain the modulation frequency 124 ps^{-1} corresponding to the resonant frequency of the Raman vibrational mode 655.7 cm^{-1} and the standard deviation 0.107 cm^{-1}.

We have studied the higher-order correlation effects on the REPB using three types of stochastic models. The overall accuracy of using broadband REPB to measure the Raman resonant frequency is also considered. Polarization beats can be employed as a spectroscopy because the modulation frequency corresponds directly to the resonant frequency of the system [15]. For the Raman resonant system, the modulation frequency is just the frequency difference of the two incident lasers when the

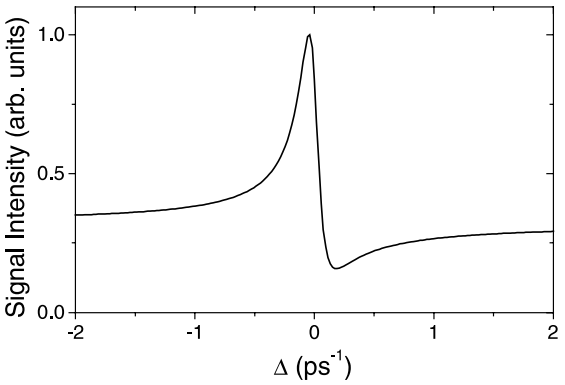

Fig. 7. RENFWM spectrum with fixed time delay.

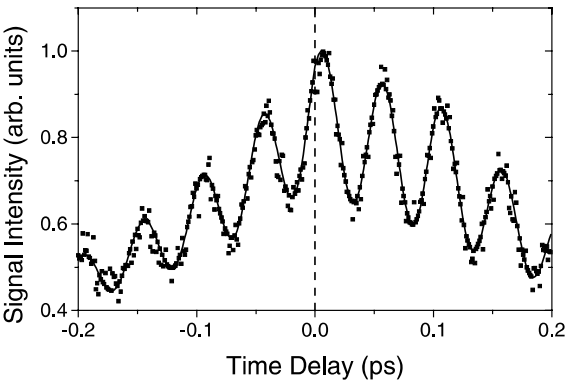

Fig. 8. The beat signal intensity versus relative time delay. The filled squares denote the experimental result; the solid curve is the theoretical curve with $\omega_1 = 3200$ ps^{-1}, $\omega_3 = 3324$ ps^{-1}, $\Delta k = 0$, $\eta_1 = \eta_2 = 1$, $\delta\tau = 83$ fs, $\Delta = 0$, $\chi/\chi_R = 1$, $\gamma_R = 0.05$ ps^{-1}, $\gamma = 0.2$ ps^{-1}, $\alpha_1 = 2.7$ ps^{-1} and $\alpha_3 = 2.9$ ps^{-1}.

lasers have narrow bandwidths. The precision of using REPB to measure the Raman resonant frequency is then determined by how well $\omega_3 - \omega_1$ can be tuned to Ω_R. However, due to the interference between the Raman resonant signal and the nonresonant background, the Raman enhanced FWM signal spectrum is asymmetric and the peak of the spectrum does not correspond to the exact Raman resonant. Since there is a small uncertainty on tuning $\omega_3 - \omega_1$ to Ω_R, there is disadvantage of using narrow band polarization beat to measure the resonant frequency of the Raman mode [9]. On the contrary, since the modulation frequency of the beat signal corresponds directly to the Raman resonant frequency when the lasers have broadband linewidths, there is great advantage of using broadband polarization beat to measure the resonant frequency of the Raman mode. In this paper, we present a theory and experimental results for the material response in REPB with phase-conjugation geometry using broadband chaotic fields, which can provide Raman frequencies, is another interesting way to study the stochastic properties of light. Previous extensive noisy light based CRS often called $I^{(2)}$ CARS or $I^{(2)}$ CSRS (coherent Stokes Raman scattering) yield both Raman frequencies via radiation difference

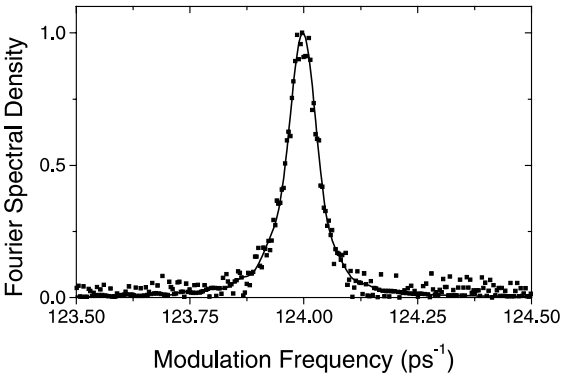

Fig. 9. The filled squares denote the Fourier spectrum of the experimental data in which τ is varied for a range of 5 ps. The solid curve is the theoretical curve with $\omega_1 = 3200\ \text{ps}^{-1}$ $\omega_3 = 3324\ \text{ps}^{-1}$, $\Delta k = 0$, $\eta_1 = \eta_2 = 1$, $\delta\tau = 83$ fs, $\Delta = 0$, $\chi/\chi_R = 1$, $\gamma_R = 0.05\ \text{ps}^{-1}$, $\gamma = 0.2\ \text{ps}^{-1}$, $\alpha_1 = 2.7\ \text{ps}^{-1}$ and $\alpha_3 = 2.9\ \text{ps}^{-1}$.

oscillations (RDOs) and dephasing times in the interferometric time domains. Unlike in REPB in those spectroscopies the presence of one monochromatic beam is essential [11–14]. Physically the REPB is similar to the corresponding CSRS [23–25].

The temporal behavior of the REPB signal is quite asymmetric with the maximum of the signal shifted from $\tau = 0$. We attribute this asymmetry to the difference between two autocorrelation processes in the zero time delay. To confirm this, we can measure the FWM signal when beams 1 and 2 only consist of only one frequency component. The difference in the zero-time delay was obvious in that figure [22]. It is due to the large difference between the wavelengths of broadband noisy light sources DL1 and DL2 so that the dispersion of the optical components becomes important. This can be understood as follows. The correlation functions of static gratings G1 and G2 is chirped in these experiments owing to unbalanced dispersion in the interferometer generated by a dispersive material (the optical glass in the delay line) in one arm but not the other. Owing to the difference in the indices of refraction of optical glass and air, the beam 2 is delayed by the optical glass relative to beam 1. Therefore the interferometer must be adjusted (the path of beam 2 is made shorter) to match this delay and thus reestablish overlap, defined as that interferometric delay setting which allows for the global minimization of the difference in phases of all of the colors contained in beam 1 relative to the same colors in beam 2. The difference between the dispersion of optical glass and air causes chirping of the correlation function, so different colors are optimally correlated at different values of the interferometric delay. The bluer color ω_3 correlate at later delay times (when the path of beam 2 is made shorter) and the redder color ω_1 correlate at earlier delay times (when the path of beam 2 is made longer) [11,14]. Consider the case that the optical paths between 1 and 2 are equal for ω_3 component. Owing to the difference between the zero time delays for the frequency components ω_1 and ω_3, the optical paths between beams 1 and 2 will be different by $c\delta\tau$ for the ω_1 component. As the result, there is an extra phase factor $\omega_1\delta\tau$ for the ω_1 frequency component. For an optical glass with refractive index $n \approx 1.5$, the refractive index at $\lambda_3 = 567$ nm is larger than that at $\lambda_1 = 589$ nm by approximately 0.001. A 83 fs delay between ω_1 and ω_3 corresponds to the propagation of beams in the glass (mainly the prism in the optical delay line) for a distance of about 2.5 cm. It is worth mentioning that the asymmetric behaviors of the polarization beat signals due to the unbalanced dispersion effects of the optical components between two arms of interferometer do not affect the overall accuracy in case using REPB to measure the energy-level difference. By contrast, ultrashort pulses of equivalent bandwidth are not immune to such dispersive effects (even when balanced) because the transform limited light pulse is in fact

temporally broadened (it is chirped) and this has drastic effects on its time resolution (the auto-correlation). In this sense the REPB with broadband noisy light has an advantage [11].

In conclusion, the higher-order field correlation effects on the REPB with phase-conjugation geometry in Raman resonant system are investigated using chaotic field, phase-diffusion, and Gaussian-amplitude models. The polarization beat signal is shown to be particularly sensitive to the field statistics. Different stochastic models of the laser field only affect the sixth- and fourth-order coherence function. Based on three types of models, the cases that the pump beams have either narrow band or broadband linewidths are considered, and it is found that the beat signal oscillates not only temporally with a period of 51 fs but also spatially with a period of 0.6 mm. The temporal period corresponds to the Raman frequency shift of 655.7 cm^{-1}. The overall accuracy of using REPB to measure the resonant frequency of Raman-active mode is determined by the relaxation rates of the Raman mode and the molecular-reorientational grating. It is worth mentioning that the asymmetric behaviors of the polarization beat signals due to the unbalanced dispersion effects between two arms of interferometer do not affect the overall accuracy in case using REPB to measure the Raman resonant frequency, and different colors are optimally correlated at different values of the interferometric delay.

Acknowledgements

This work was supported by the Chinese National Nature Sciences Foundation (Grant No. 69978019) and the State Key Laboratory Foundation of Transient Optics Technology (Grant No. YAK20006).

References

[1] A.T. Georges, Phys. Rev. A 21 (1980) 6.
[2] R.E. Ryan, T.H. Bergeman, Phys. Rev. A 43 (1991) 6142.
[3] C. Chen, D.S. Elliott, M.W. Hamilton, Phys. Rev. Lett. 68 (1992) 3531.
[4] M.H. Anderson, G. Vemuri, J. Cooper, P. Zoller, S.J. Smith, Phys. Rev. A 47 (1993) 3202.
[5] R. Bratfalean, P. Ewart, Phys. Rev. A 56 (1997) 2267.
[6] Y.P. Zhang, T.T. Tang, L.Q. Sun, P.M. Fu, Phys. Rev. A 61 (2000) 023809.
[7] Y.P. Zhang, L.Q. Sun, T.T. Tang, P.M. Fu, J. Opt. Soc. Am. B 17 (2000) 690.
[8] Y.P. Zhang, L.Q. Sun, T.T. Tang, L. Zhang, P.M. Fu, Chin. Phys. Lett. 17 (2000) 206.
[9] Y.P. Zhang, X. Hou, K.Q. Lu, H.C. Wu, Opt. Commun. 184 (2000) 265.
[10] Y.P. Zhang, K.Q. Lu, C.S. Li, X. Hou, C.B. de Araujo, J. Mod. Opt. 48 (2001) 549.
[11] D.C. DeMott, D.J. Ulness, A.C. Albrecht, Phys. Rev. A 55 (1997) 761.
[12] D.J. Ulness, A.C. Albrecht, J. Raman Spectrosc. 28 (1997) 571.
[13] M.J. Stimson, D.J. Ulness, A.C. Albrecht, J. Raman Spectrosc. 28 (1997) 579.
[14] M.J. Stimson, D.J. Ulness, J.C. Kirkwood, G.S. Boutis, J. Opt. Soc. Am. B 15 (1998) 505.
[15] D. DeBeer, L.G. Van Wagenen, R. Beach, S.R. Hartmann, Phys. Rev. Lett. 56 (1986) 1128.
[16] H. Ma, A.S.L. Gomes, C.B. de Araujo, Opt. Lett. 17 (1992) 1052.
[17] P.M. Fu, X. Mi, Z.H. Yu, Q. Jiang, Y.P. Zhang, X.F. Li, Phys. Rev. A 52 (1995) 4867.
[18] Y.P. Zhang, C.B. De Araújo, E.E. Eyler, Phys. Rev. A 63 (2001) 043802.
[19] Y.P. Zhang, T.T. Tang, S. Li, L.Q. Sun, Acta Phys. Sin. 48 (1999) 1452.
[20] Y.P. Zhang, C.L. Gan, J.P. Zhu, T.T. Tang, P.M. Fu, Acta Phys. Sin. 48 (1999) 1667.
[21] Y.P. Zhang, K.Q. Lu, H.C. Wu, J. Xu, P.M. Fu, Chin. Phys. 9 (2000) 606.
[22] Y.P. Zhang, L.Q. Sun, T.T. Tang, P.M. Fu, Phys. Rev. A 61 (2000) 053819.
[23] P.M. Fu, Z.H. Yu, X. Mi, Q. Jiang, Z.G. Zhang, Phys. Rev. A 46 (1992) 1530.
[24] X. Mi, Z.H. Yu, Q. Jiang, P.M. Fu, Phys. Rev. A 48 (1993) 3203.
[25] Z.H. Yu, X. Mi, Q. Jiang, X.F. Li, P.M. Fu, Phys. Rev. A 55 (1997) 2334.
[26] Y.P. Zhang, H.C. Wu, P.F. Wang, C.S. Li, P.M. Fu, Chin. Phys. 9 (2000) 599.
[27] N. Morita, T. Yajima, Phys. Rev. A 30 (1984) 2525.

[28] S. Asaka, M. Nakatsuka, M. Fujiwara, M. Matsuoka, Phys. Rev. A 29 (1984) 2286.
[29] D.V. Bout, M. Berg, J. Raman Spectrosc. 26 (1995) 503.
[30] A. Tokmakoff, G.R. Fleming, J. Chem. Phys. 106 (1997) 2569.
[31] R. Trebino, E.K. Gustafson, A.E. Siegman, J. Opt. Soc. Am. B 3 (1986) 1295.